Accepted Manuscript

Onset of foreland basin deposition in the Neuquén Basin (34°-35°S): New data from sedimentary petrology and U–Pb dating of detrital zircons from the Upper Cretaceous non-marine deposits

Ricardo Gómez, Lucas Lothari, Maisa Tunik, Silvio Casadio

PII: S0895-9811(19)30043-4

DOI: https://doi.org/10.1016/j.jsames.2019.102257

Article Number: 102257

Reference: SAMES 102257

To appear in: *Journal of South American Earth Sciences*

Received Date: 22 January 2019

Revised Date: 25 June 2019

Accepted Date: 1 July 2019

Please cite this article as: Gómez, R., Lothari, L., Tunik, M., Casadio, S., Onset of foreland basin deposition in the Neuquén Basin (34°-35°S): New data from sedimentary petrology and U–Pb dating of detrital zircons from the Upper Cretaceous non-marine deposits, *Journal of South American Earth Sciences* (2019), doi: https://doi.org/10.1016/j.jsames.2019.102257.

This is a PDF file of an unedited manuscript that has been accepted for publication. As a service to our customers we are providing this early version of the manuscript. The manuscript will undergo copyediting, typesetting, and review of the resulting proof before it is published in its final form. Please note that during the production process errors may be discovered which could affect the content, and all legal disclaimers that apply to the journal pertain.

ACCEPTED MANUSCRIPT

Onset of foreland basin deposition in the Neuquén Basin (34°-35°S): new data from sedimentary petrology and U-Pb dating of detrital zircons from the Upper Cretaceous non-marine deposits

Ricardo Gómez*, Lucas Lothari, Maisa Tunik, Silvio Casadio

Instituto de Investigaciones en Paleobiología y Geología (CONICET-UNRN), Ave. Roca 1242, General Roca, Río Negro, Argentina

*Corresponding author e-mail: rgomez@unrn.edu.ar

Abstract

A multi-proxy provenance approach using sedimentology, petrology and detrital zircon U–Pb geochronology provides new constrains for the evolution of the Southern Central Andes. The Upper Cretaceous non-marine deposits of the Neuquén Basin referred as Neuquén Group in the central and southern sector of the basin, have been characterized as the first foreland basin associated with the early uplift of the Andean orogen at ca. 100 Ma. However, in the northern sector of the basin, the stratigraphically equivalent Diamante Formation has not been studied in detail yet. This work focuses in the outcrops of the Diamante Formation located between Laguna del Diamante and Atuel River in southern Mendoza Province, Argentina (34°-35°S). The petrographic analysis of sandstones shows high content of volcanic and calcareous lithic fragments suggesting provenance from the underlying sedimentary units and the coeval volcanic arc associated with the onset of an important stage of deformation on the west. Detrital zircons from the base of the Diamante Formation were supplied sources from Upper Jurassic and Lower Cretaceous that were exposed during Upper Cretaceous times, whereas in the top, a high content of Permo-Triassic detrital zircons indicates

exhumation of the surrounding Permo-Triassic crystalline basement. Finally, two maximum depositional ages were obtained, 107.2±1.4 Ma to Vega de los Patos and 91.1±2.2 Ma to Vega Grande, suggesting uninterrupted activity of the volcanic arc during foreland basin deposition. In particular, the age of 107.2 Ma would indicate that the sedimentation of the Upper Cretaceous non-marine deposits occurred in the Albian at these latitudes (34°-35°S), which suggests that the onset of the foreland basin sedimentation is diachronic at different positions in the Neuquén Basin.

1. Introduction

For several years, the Upper Cretaceous non-marine deposits in the Neuquén Basin have been studied in order to understand the early uplift history of the Andean orogen using sedimentological, structural and provenance analyses. However, in the last couple of years, thermochronology and geochemistry have been added to constrain uplift and crustal shortening phases mainly at the central Neuquén and southern Mendoza provinces (Zamora Valcarce et al., 2009; Garrido, 2010; Tunik et al., 2010; Di Giulio et al., 2012, 2016, Balgord and Carrapa, 2016; Fennell et al., 2017a, 2017b; Asurmendi et al., 2017; Balgord, 2017; Folguera et al., 2015; Rojas Vera et al., 2014). The outcrops are largely developed in the San Juan, Mendoza, Neuquén and Río Negro provinces, Argentina, reaching 1.600 m in some areas (Orts et al., 2012). According to several authors, those rocks are Cenomanian-Campanian in age (Legarreta and Gulisano, 1989) and are known as the Neuquén Group south of 35°S (see Garrido, 2010 for more details). North of 35°S these are known as Diamante Formation and their age seems to be Albian-Santonian (Mackaman-Lofland et al., 2019). Previous studies in central Neuquén and southern Mendoza provinces indicate that before the uplift of the Andes, positive areas were located towards the east behaving as source regions for

fluvial systems and perennial lakes, represented by the sediments of the Bajada del Agrio Group (Zavala et al. 2001, 2006; Ponce et al. 2002; Tunik et al., 2010). The Bajada del Agrio Group was formalized by Leanza (2003) to include the Huitrín and Rayoso formations, while the Diamante Formation was initially defined by Groeber (1946) to include all the reddish nonmarine deposits overlying the Huitrín Formation in Mendoza Province, which have not been studied in detail since then. The reasons why the authors of this manuscript decided to use the name of Diamante Formation instead of Neuquén Group are related to the discrepancy that was generated from the different background and parameters that were taken into account to correlate the units at a regional-level based on the absence of guide levels and fossil content. It is not possible to detect the same facies arrangement and divide the unit into subgroups or formations compared to the central-southern sector of the Neuquén Basin. However, the age of detrital zircons is an important tool to demonstrate a correlation between the nonmarine deposits outcropping in the Mendoza Province and the Neuquén Group defined further south. In consequence, the authors of this manuscript considered the Diamante Formation as a temporary equivalent of the Neuquén Group because of the stratigraphic position and the ages of detrital zircons.

Detrital zircon U–Pb geochronology has become a common tool in the last couple of years to obtain maximum sedimentation ages and characterize the provenance of sedimentary units. This study aims to determine the timing, depositional environments and source areas of foreland basin deposits in the northern sector of the Neuquén Basin from a multidisciplinary approach that combines sedimentology, petrology and detrital zircon U–Pb geochronology of the Diamante Formation in the localities of Vega Grande and Vega de los Patos, located in the central-western sector of the Mendoza Province, Argentina (Fig. 1).

2. Geological setting

The study area is located in the central-western sector of the Mendoza province, in the geological province of the Principal Cordillera (Turienzo, 2009) and more specifically in the Malargüe fold- thrust belt (Kozlowski et al., 1993; Manceda and Figueroa, 1995) (Figs.1-2), approximately 120 km west of the San Rafael city and 13 km from the Las Aucas village.

The Malargüe fold-thrust belt exposes sediments of the Neuquén Basin, on the eastern slope of the Andes in Argentina, between 32° and 40°S (Fig. 1). This basin comprises a continuous sedimentary record from the Late Triassic to the Early Cenozoic and includes non-marine and marine siliciclastics, carbonates and evaporites that accumulated under a variety of basin styles (Howell et al., 2005). It is bounded towards the northeast by the San Rafael Block and towards the southeast by the North Patagonian Massif, while its western margin corresponds to the Mesozoic magmatic arc (Fig. 1) (Howell et al., 2005; Charrier et al., 2007, 2014).

The opening of the Neuquén Basin is related to extensional processes occurred in a retroarc position starting in Late Triassic times, which coexisted with minor tectonic inversion episodes in the Huincul ridge during the Jurassic-Cretaceous interval (Vergani et al., 1995; Howell et al., 2005; Silvestro and Zubiri, 2008; Armas and Sanchez, 2013 among others). Since the Late Cretaceous, as a consequence of the Andean uplift, the Neuquén Basin evolved into a typical foreland basin, whose base defines a regional unconformity with the underlying sediments (Cazau and Uliana, 1973; Ramos, 1999; for a summary, see Garrido, 2010).

The transition into a foreland basin begins at the end of the Early Cretaceous with a slab shallowing event, producing a shift towards a compressive tectonic regime

and causing the migration of the orogenic front towards the east (Gianni et al., 2018). Provenance analyses and detrital zircons U-Pb age patterns suggest that the foreland basin was established in the retroarc at approximately 100 Ma with the deposition of Neuquén Group or Diamante Formation (Tunik et al., 2010, Di Giulio et al., 2012, 2016, Balgord and Carrapa, 2016 and Fennell et al., 2017a).

The Upper Cretaceous Andean foreland basin comprises a stratigraphic record of synorogenic sediments, referred as Neuquén Group in the central and southern areas of the Neuquén Basin, and Diamante Formation in the northern area. The Neuquén Group comprises a thick non-marine succession and is subdivided into three subgroups (Río Limay; Río Neuquén; and the Río Colorado) and seven formations: Candeleros, Huincul and Cerro Lisandro formations in the Río Limay Subgroup; Portezuelo and Plottier formations in the Río Neuquén Subgroup; Bajo de la Carpa and Anacleto formations in the Río Colorado Subgroup (Cazau and Uliana, 1973; Uliana et al., 1975; Ramos, 1981; Leanza and Hugo, 2001; Leanza et al., 2004; Garrido, 2010). The formations within this unit record a cyclic repetition of medium- to coarse grained facies, interpreted as braided and meandering fluvial channels, fine-grained alluvial plain deposits with intercalations of aeolian systems and shallow lakes (Legarreta and Uliana, 1998; Garrido, 2010). This cyclic pattern is interrupted by the overlying Maastrichtian - Palaeocene marine facies of the Malargüe Group (Uliana and Dellapé, 1981; Barrio, 1990; Aguirre-Urreta et al., 2008). On the other hand, the Diamante Formation is informally divided into three members according to Balgord and Carrapa (2016) broadly correlated with the Río Limay, Río Neuquén and Río Colorado subgroups from the Neuquén Group. On the base, the unconformity that separates the Bajada del Agrio Group from the base of the Neuquén Group corresponds to a basin-scale angular unconformity (Leanza, 2003, 2009; Mosquera and Ramos, 2006).

However in our study area this unconformity is not represented, being the contact between the Bajada del Agrio Group and the Diamante Formation transitional (Lothari et al., 2018).

Based on paleomagnetic studies, Dingus et al. (2000) estimated the age of the Anacleto Formation (top of the Neuquén Group) as early Campanian (~ 83.5-79.5 million years old). In the southern part of the Neuquén Basin, in the Cerro Policía site (39ºS), Corbella et al. (2004) obtained a zircon fission-track age of 88±3.9 Ma (Coniacian) for a tuff interbedded in the lower section of the Neuquén Group, which confirms the Late Cretaceous age of this unit. However, the absence of radiometric ages on volcanic levels interbedded in the Neuquén Group impedes to obtain an absolute age of this unit.

3. Methods

A detailed stratigraphic study along with provenance analyses based on sedimentary petrography were combined with U–Pb detrital zircon geochronology of samples collected from the Diamante Formation in outcrops located between the Río Diamante and Río Atuel (34°30'-34°50'S).

Sedimentology

The stratigraphic analysis of the non-marine Upper Cretaceous succession was carried out based on the description of two stratigraphic sections (Fig. 3-4) of metric scale. This analysis included a detailed description of outcrops and measurements using Jacob's staff. This allowed the characterization of sedimentary facies based on lithology (including texture and composition), sedimentary structures (types, dimensions and orientation in case of having directional character) and internal organization. The system used to denominate sedimentary facies was based on Miall (1996), with slight

modifications. This information allowed the definition of facies and facies associations, which were interpreted to propose a paleoenvironmental model of the Diamante Formation in this sector of the basin.

Petrography

A systematic sampling of sandstones was carried out based on two detailed stratigraphic sections from Vega Grande and Vega de los Patos locations (Fig. 3-4), which were observed under a magnifying glass for a complete macroscopic description. Standard 30 microns thin sections were impregnated with blue epoxy resin in order to highlight the porosity, stained with alizarin red to distinguish dolomite and calcite and also with potassium ferricyanide to distinguish ferroan and non-ferroan calcite following the method of Dickson (1965). After analyzing the sections under a petrographic microscope, 10 samples from Vega Grande area and 8 from Vega de los Patos were selected for the study of detrital modes and provenance (Appendix 1). The sandstones were classified following Folk et al. (1970) and the Gazzi-Dickinson method was used for the provenance analyses based on a 400 clasts count for each thin section (Ingersoll et al., 1984). All the data was later included in the Dickinson et al. (1983) discrimination provenance diagrams.

U-Pb detrital zircon geochronology

A sample of a re-worked tuff located on the top of the Vega Grande section was collected (VG24-16) for the separation and U-Pb dating of detrital zircons. This re-worked tuff level is 50 cm thick, massive, friable, white to grey and appears below a floodplain deposit with paleosol development. Another sample of medium-grained lithic feldespathic sandstone was collected from the base of the Vega de los Patos section (VLP001-17), close to the contact with the Rayoso Formation (Bajada del Agrio Group).

The separation of zircons was carried out in two stages. The first was carried out at the Instituto de Investigación en Paleobiología y Geología (CONICET-UNRN). In this place, standard separation techniques were used, which consist of milling, sieving and subsequent concentration by hydraulic methods of heavy minerals. Those heavy minerals were later observed under a magnifying glass to confirm the presence of zircons. During the second stage, the concentration of heavy minerals was sent to the Arizona LaserChron Center of the Arizona University, where the separation of zircons was first performed using heavy liquids and Frantz separator. Finally, the U-Pb dating of detrital zircons was conducted by laser ablation multicollector inductively coupled plasma mass spectrometry (LA-MC-ICPMS), based on the methodology and analytical data proposed by Gehrels et al. (2006, 2008). For details in the methodology and analytical data see Appendix 2.

4. Results

4.1. Facies Analysis

In the area of Vega Grande (Fig. 6B), the Diamante Formation has a thickness of 377 m, presents a covered base and towards the top shows a change from red-mudstones to laminated green and yellow siltstones and shales (Fig. 5A) marking a transitional passage towards marginal marine deposits of the Saldeño Formation (Tunik, 2001). In this area, the unit is divided into two upward fining and thinning sequences (Fig. 3). Nine facies and two facies associations - Channels and Bars (FAI) and the Floodplain (FAII) – were established in this area (Gómez et al., 2016a, 2016b).

In Vega de los Patos area, the contact between the Rayoso and Diamante formations is semi-covered with a transitional passage marked by a change from thinly laminated-mudstones with minor interbedded gypsum (Fig. 5B-C) to medium-

sandstones and conglomerates without gypsum and with lenticular geometries (Fig. 5D) showing a clear change in the paleoenvironmental conditions. Fifteen sedimentary facies and five facies associations were analyzed and interpreted; A: restricted brackish lake; B: ephemeral lake; C: terminal lobes; D: high-sinuosity channels and E: braided-channels (Fig. 4). The analysis of facies associations and their spatial arrangement allowed the detection of two depositional sequences: S1 and S2. Both sequences have similar thickness (S1: 305 m; S2: 280 m). S1 and S2 are composed of the organized sequence of facies associations C, D and E. This arrangement in the sedimentary succession marks cyclicity in stacking patterns showing a change regarding associations A and B located toward the base of the section. However, contact between associations B and C is transitional. In this area, the measured thickness of the Diamante Formation is 565 m (Lothari et al., 2018).

In both areas, paleocurrent data is limited, due to the absence of measurable sedimentary structures and the scarce levels with imbricated clasts.

Another important feature is the presence of conglomerates at the top of both stratigraphic sections composed almost exclusively of carbonate fragments (Fig. 6D) with ammonites.

4.2. Sandstone Petrography

The Upper Cretaceous sandstones of the Diamante Formation in the area of Vega de los Patos and Vega Grande are mainly feldspatic litharenites, on average $Q_{44}F_{18}L_{38,}$ and scarce litharenites, on average $Q_{37}F_{13}L_{50}$ (Appendix 1-Fig. 8A), with percentages of matrix below 10%.

The average quartz proportion in the samples is of 42% and the predominant variety is monocrystalline with straight extinction (Fig. 7). Quartz with undulatory

extinction (5.2%) was also recognized, as well as quartz as a fragment of a volcanic rock (on average 5%). Embayment quartz with volcanic matrix preservation was observed. Within the analyzed stratigraphic section, a clear tendency to increase the quantity of quartz towards the top can be observed, with values of 33% in the bottom of Vega de los Patos to 55% in the upper part of Vega Grande. The polycrystalline quartz (on average 6.7%) is relatively low in all the section.

Regarding alkaline feldspar and plagioclase, the average proportions are of 8% and 6.1% respectively, and normally present sericitic and argillic alteration. In addition, alkaline feldspar and plagioclase (on average 2.5%) were recognized as volcanic rocks crystals and in some cases replaced by calcite (Fig. 7).

The lithic fragments make up for 42% of the clastic fraction, a high average percentage compared to the quartz and feldspar (Fig. 7). This characteristic was also noticed by Balgord and Carrapa (2016) for the Diamante Formation located around 100 km to the south. The lithic fragments are angular to subangular and present themselves in various ranges of sizes, and belong to volcanic rocks, more specifically to the paleovolcanic type according to Critelli and Ingersoll (1995). In almost all the samples, fragments of volcanic rocks with felsitic, granular, micro granular and seriate textures are predominant, although volcanic fragments with pilotaxic and pyroclastic texture were also observed. In addition, high proportions (34.5%) of calcareous lithic fragments in the mid part of the section (sample VG16) were recognized (Fig. 7C). A large amount of altered lithic fragments and pseudomatrix (VG2) was also identified. Sedimentary lithic grains, metamorphic rock fragments and plutonic lithic clasts were observed as well in very low proportions (less than 2%).

The most common type of cement is the calcareous, followed by zeolitic, ferruginous and argillaceous type. The cement appears as pore filling, pore lining and

ACCEPTED MANUSCRIPT

scarce poikilotopic (Fig. 7). The alizarine red and potassium ferricyanure stain allowed establishing that carbonate cement is non-ferrous calcite. The average percentage of zeolitic cement within the samples is low (2%), but in some samples like VG9 and VG8 the percentage rises due to the presence of analcime which occurs as pore filling cement and in subhedral crystals related to calcite cementation (Fig. 7).

4.3. Provenance

4.3.1. Point counting

In this study the sandstones modal analysis is used to characterize the input area. The recalculated modal composition for the sandstones (Appendix 1) was plotted on the provenance graphs of Dickinson et al. (1983). The Qt-F-Li graph indicates that the analyzed samples mostly fall in the recycled orogen field and few in dissected arc field (Fig. 8B). This variation correlates with the stratigraphic position of the samples, with the dissected arc field samples belonging to the base of the Vega de los Patos section, while samples falling inside the recycled orogen field belong to the top of Vega Grande section. On the other hand, the Qm-F-Lt graph (Fig. 8B) shows a more irregular distribution of the samples, mostly falling in the transitional recycled field and the others being distributed in four fields; mixed, dissected arc, transitional arc and lithic recycled. For details in the analytical data see Appendix 1.

4.3.2. Detrital Zircon Analysis

Two samples from the Diamante Formation were analyzed for detrital zircon U-Pb geochronology (Table 1A-B-Appendix 2). Frequency histograms, relative probability plots, and concordia plots of U–Pb ages from analyzed zircons are shown in Fig. 9.

The sample from Vega Grande section corresponds to a reworked tuff (VG24-16, n=187) and is located at the top of the section (34°40'18.56"S; 69°40'3.32"W), near to the contact with the Saldeño Formation. 187 U-Pb ages were determined, presenting their distribution a multimodal pattern (Table 1). This sample is dominated by three major age populations, 250-300 Ma (50%), 900-1200 Ma (20%) and 500-600 Ma (11%), with minor peaks that correspond to the youngest zircons of Cretaceous age (4%), as well as those of Early Paleozoic age (4%), Mesoproterozoic (7%), Paleoproterozoic (3%), and even a zircon of Neoarchaean age (1%) (Fig. 9A-C).

On the other hand, a sample of litharenite (VLP001-17, n=212) from the base of Vega de los Patos section (Lothari et al., 2018), near to the contact with the Bajada del Agrio Group (34°39'31.04"S, 69°41'33.68"O), three main peaks can be distinguished; 250-365 Ma (32%), 500-700 Ma (21%) and 100-153 Ma (23%) (Table 1). The difference between the age distribution of both samples (VG24-16 and VLP001-17), is the peak of young ages. In the case of this last sample, the population of younger ages is greater, including Cretaceous and Late Jurassic ages, while the other two peaks are repeated in both samples with different percentages (Fig. 9B-D).

4.4. Maximum Depositional Age

Both samples contain distinct young zircon U/Pb age clusters that may be used to infer the maximum depositional age of the sample.

For the calculation of the maximum depositional age, different ways of measurement were considered, from the most robust to the least robust from the statistical point of view (Dickinson and Gehrels, 2009). As a result of data analysis, weighted mean average of the youngest cluster of two or more grain ages that overlap at 1σ uncertainty, was the estimation that was better adjusted for the samples of the

Diamante Formation. The ages also overlap with the TuffZirc age, especially in the sample VG24-16, since in the sample VLP001-17 it does so with certain uncertainty. TuffZirc age is an algorithm defined by Ludwig and Mundil (2002) for the youngest cluster of coherent grain ages. Finally, the authors decided to use the first estimation since the error is smaller (1σ), while in the TuffZirc algorithm the uncertainty is greater (2σ). The analytical details are provided in the appendix.

The sample of reworked tuff (VG24-16) from the top of Vega Grande section, yields a maximum depositional age of 91.1±2.2 Ma (1σ;n=3) (Fig. 10A), while the sample of litharenite from the lower portion of the Vega de los Patos section, yields a maximum depositional age of 107.2±1.4 Ma (1σ;n=4) (Fig. 10B).

5. Discussion

5.1. Importance of lithic fragments composition

The petrographic analysis suggests that the composition and proportion of lithic fragments in the Upper Cretaceous sandstones is not only associated with the nature and tectonic history of the source area, but also reflects particular transport and weathering, which can be interpreted as semi-arid due to the high amount of lithic fragments (Potter, 1994). The presence of embayments on the quartz supports active volcanic processes, while the presence of analcime as cement (sample VLP01, VLP02, VLP03, VLP05, VG1 and VG9) indicates volcanic glass alterations. The latter presents itself filling pores, completely sealing the porosity present. The volcanic lithic fragments with felsitic textures could derive from uplift and erosion of the San Rafael Block to the east-northeast (Kleiman and Japas, 2009) as well as from Late Jurassic-Early Cretaceous extensive bimodal magmatic activity to the west (Vergara et al., 1995). Based on the geological context of the area and the presence and proportion of a high content of

volcanic lithic fragments with pilotaxic and pyroclastic textures, which indicate the erosion of a volcanic arc, along with the presence of calcareous lithic fragments (sample VG16), provenance from the western Andean orogen is clear. This suggests a stage of active deformation and exhumation in the area. In reference to the latter, Tunik (2001) mentioned the presence of limestone clasts in the Diamante Formation about 20 km northwest from the study area while describing the general overview of the unit. On the other hand, Borghi et al. (2017) described fragments of limestone in conglomerates of Neuquén Group to the south of the study area while Balgord and Carrapa (2016) described, in an area near the locality of Malargüe, a change in sandstone composition within the Diamante Formation, from volcanic lithic on the base (lower Diamante Formation) to a higher content of sedimentary lithic fragments towards the mid and upper parts (middle and upper Diamante Formation). These authors interpreted this sandstone composition variation as a change in the source area, first from the east and then from the west, based on the migration of the forebulge, product of the eastward migration of the fold-thrust belt front. It is important to consider that the volcanic rock fragments could be associated with the erosion of the San Rafael Block, another positive area located towards the east. Noteworthy, input from both magmatic arcs and recycled orogen is a common feature in foreland basins, especially in orogenic systems involving active magmatic arcs (Scasso and Limarino, 1997). In these conditions, the detrital modes will reflect, just as Dickinson et al. (1983) diagrams show, transitional characteristics within the field of recycled orogen.

5.2. Upper Cretaceous active volcanism (34-35°S)

The presence of at least two thick levels of reworked tuffs in the Vega Grande area fall in agreement with the existence of active volcanism near the area during Late Cretaceous times. Recently, Muñoz et al. (2018) at ~ 35°S provided new evidence of

Cretaceous volcanic activity in the Chilean Andes and their relation with BRCU (Brownish Red Clastic Unit), a unit correlated with the Neuquén Group in Argentina. According to these authors, the Plan de los Yeuques Formation represents the Upper Cretaceous (Campanian-Danian) coeval magmatic arc at this latitude of the Chilean Coastal Cordillera. These events represent a bimodal volcanic suite and extended at least between the early Campanian and Danian (~ 80-63 Ma). This is coherent with the presence of acid and mafic lithic volcanic fragments in samples of the Diamante Formation at ~ 34°S (Argentina) and could be the source of detrital zircons <100 Ma (~ 92-80 Ma) from Vega Grande sample (VG24-16).

5.3. Significance of geochronological data

According to the frequency diagram of detrital zircon ages, obtained from VG24-16 sample analysis, a multimodal pattern of ages can be distinguished. One of the main age peaks corresponds to Gondwanic ages, especially Permian ages. Those ages are related to the Choiyoi Magmatic Province (Kay et al., 1989) and Precuyano cycle rocks exposed both to the east (San Rafael Block) and north-east of the study area (Frontal Cordillera). Therefore, taking into account the scarce information of paleocurrents in this section, the source area is uncertain since there are multiple possibilities. Another important peak of zircon ages is the Neoproterozoic-Lower Cambrian peak derived from Pampean magmatism (500-600 Ma), exposed in outcrops located to the east of the study area (Ramos, 2010). The Meso-Neoproterozoic-aged zircon grains, representing 20% of the total sample, could be derived either from the Grenville basement (900-1250 Ma) of the Chilenia terrane in Frontal Cordillera (Ramos and Basei, 1997) or from the basement of the Cuyania terrane in the San Rafael Block (Cingolani et al., 2005; Thomas et al., 2012) located northeast and east of the study area, respectively. The zircons of Cretaceous age (n = 8) represent 4% of the total

percentage of the sample (n = 187) and have ages ranging from 81.5 to 112.5 Ma. The latter, despite being scarce, supports the contribution from the Cretaceous Andean arc (Tunik et al., 2010) located to the west. Moreover, the presence of youngest zircons in VG24-16 sample (e.g. 81.5 Ma) represents a difference with detrital zircon data from the upper Neuquén Group in others parts of the Neuquén Basin (Fennell et al., 2017a; Balgord and Carrapa 2016; Di Giulio et al., 2012; Tunik et al., 2010), where detrital zircons younger than 100 Ma are absent. This absence has been interpreted as the result of the growth of the fold and thrust belt inhibiting the sediment supply from the Cretaceous magmatic arc located in the current Coastal Cordillera, Central Depression and Western Principal Cordillera (Muñoz et al., 2018) or to a decline in arc activity between ca. 100 and 85 Ma (Fennell et al., 2017a; Balgord, 2017). Probably, the presence of youngest zircons in the Vega Grande sample, which can be derived either from: (i) the recycling of Upper Cretaceous sedimentary deposits located on the topographic barrier, (ii) the transport of volcanic material located in the back-arc area through fluvial systems or (iii) the presence of air-fall tuffaceous levels.

Regarding VLP001-17 sample from Vega de los Patos area, the ages of the zircons ranging from 102.5 to 153.8 Ma suggest that the source is associated with the erosion of the Andean magmatic arc located to the west (Tunik et al., 2010). The Upper Jurassic zircons ages (144.2 to 153.8 Ma) could come from either the erosion of the Late Jurassic magmatic arc (Rossel et al., 2014) and/or from the erosion of continental successions of the Tordillo Formation (Naipauer et al., 2015). On the other hand, Lower Cretaceous zircons ages (102.5 to 139.2 Ma) could come from the erosion of the Lower Cretaceous magmatic arc related to an extensional regime on western Gondwana (Ramos, 1999) and/or from the erosion of Lower Cretaceous sedimentary units of the Mendoza and Bajada del Agrio Groups (Tunik et al., 2010). In addition, an important

difference between the age peaks of both samples is that in sample VLP001-17, Grenvillian-ages zircon grains are subordinated (8%), while in sample VG24-16 they represent one of the main peaks (20%). Those zircon grains could be derived either from the Andean crystalline basement or from the Cuyania terrane (San Rafael Block) due to peripheral bulge uplift (Di Giulio et al., 2012).

The weighted mean age obtained for the youngest zircons at 91.1±2.2 Ma (1σ;n=3) from the top of the Diamante Formation in Vega Grande section and 107.2±1.4 Ma (1σ;n=4) from the base of that unit in Vega de los Patos section, indicate Turonian and Albian maximum depositional ages, respectively. The first absolute age (91.1 Ma) is very close to the only radiometric age reported for the Neuquén Group, 88±3.9 Ma, based on a fission-track analysis made on an ash-flow tuff at the base of the Huincul Formation (Corbella et al., 2004) while the second maximum depositional age (107 Ma) is more coherent with the youngest zircons age population (98.6±2.5 Ma; 100.5±2.1 Ma;104.3±2.5 Ma) described in the Candeleros Formation (base of the Neuquén Group) in the central and southern sector of the Neuquén Province (Tunik et al., 2010; Di Giulio et al., 2012) and with maximum depositional ages obtained by Fennell et al. (2017a) (100.2±2.1 Ma) and Balgord and Carrapa (2016) (97±2 Ma) in southern Mendoza Province.

6. Conclusions

The main conclusions of this study can be summarized as follows:

- The petrographic analysis shows that the sandstones of the Diamante Formation in the Vega de los Patos and Vega Grande area are mainly feldspatic litharenites (on average $Q_{44}F_{18}L_{38}$), and minor litharenites ($Q_{37}L_{13}L_{50}$) according to Folk *et al.* (1970)

classification. The source areas, according to Dickinson et al. (1983), are recycled orogen (diagram QFL) and transitional recycled (diagram QmFLt).

- The youngest U-Pb ages of detrital zircons, the petrographic features of sandstones and the composition of conglomerates suggest the presence of a coeval volcanic source located to the west during sedimentation.

-The presence of limestone fragments with ammonites in conglomerates from both study areas suggests provenance from the western Andean orogen related to the growth of the fold and thrust belt that exposed Jurassic and Cretaceous sedimentary rocks.

- The variations in the U-Pb age patterns described in this work, between the base and the top of the Diamante Formation (Vega de los Patos and Vega Grande respectively) was probably associated with an increase in the volcanic activity in the beginning of the Late Cretaceous (base of Diamante Formation) and the Andean exhumation during Albian to Campanian times (top of Diamante Formation).

- Taking into account the analysis of the U-Pb data in detrital zircons, the sample from the base of the Diamante Formation in the Vega de los Patos locality, yields a maximum depositional age of 107.2±1.4 Ma (1σ;n=4) (Albian), while the sample from the top of this unit in the Vega Grande locality, yields a maximum depositional age of 91.1±2.2 Ma (1σ;n=3) (Turonian).

- Based on the youngest detrital zircon ages obtained in this study and previous data from different sectors of the Neuquén Basin, the sedimentation of the Diamante Formation within the foreland basin started during the Albian. During this stage, the transition from an extensional back-arc setting towards a compressional retroarc foreland setting took place. This is an evidence of the diachronism in Andean uplift,

indicating that the uplift of the Andes started earlier in the northern sector of the Neuquén Basin.

Acknowledgements

This study was financially supported by UNRN-40A-321 project of the Universidad de Río Negro, Argentina, as well as by PICT 2013-0095 of the Agencia Nacional de Promoción Científica y Tecnológica (Argentina). The authors want to acknowledge Juan Ignacio Ison for the preparation of thin sections, Mavi Buhler for helping with the manuscript, Brian Mahoney for processing the zircons, Maximiliano Naipauer for helping with the U–Pb detrital zircon analyses and Phoenix Global Resources company along with the people who works in Vega Grande oil field, for their helped with logistical assistance and cooperation.

References

Aguirre-Urreta, M.B., Pazos, P.J., Lazo, D.G., Fanning, C.M., Litvak, V.D., 2008. First U–Pb SHRIMP age of the Hauterivian stage, Neuquén Basin, Argentina. Journal of South American Earth Sciences 26, 91–99.

Armas, M.P., Sánchez, M.L., 2013. Sedimentología y arquitectura de las dunas costeras de la Formación Allen, Grupo Malargüe, Cuenca Neuquina - Río Negro, Argentina. Revista Mexicana de Ciencias Geológicas 30: 65-79.

Asurmendi, E., Sánchez, M.L., Fennell, L., 2017. Neuquén Group (Upper Cretaceous): a case of underfilled-overfilled cycles in an Andean foreland basin, Neuquen basin, Argentina: Journal of South American Earth Sciences, 80, 444–459.

Balgord, E., 2017. Triassic to Neogene evolution of the south-central Andean arc determined by detrital zircon U-Pb and Hf analysis of Neuquén Basin strata, central Argentina (34°S–40°S). Lithosphere 9, 453–462.

Balgord, E.A., Carrapa, B. 2016. Basin evolution of Upper Cretaceous–Lower Cenozoic strata in the Malargüe fold-and-thrust belt: northern Neuquén Basin, Argentina. Basin Research 28 (2): 183-206.

Barrio, C.A., 1990. Late Cretaceous Early Tertiary sedimentation in a semi-arid foreland basin (Neuquén Basin, western Argentina). Sediment. Geol. 66, 255e275.

Borghi, P., Gómez Omil, R., Fennell, L., Folguera, A. y Naipauer, M., 2017. Nuevas evidencias del levantamiento del sur de los Andes Centrales (36° S) durante la depositación del Grupo Neuquén. En: XX Congreso Geológico Argentino, Libro Digital: 2932-3697.

Cazau, L.B., Uliana, M.A., 1973. El Cretácico superior continental de la Cuenca Neuquina. 5° Congreso Geológico Argentino (Carlos Paz, 1972), Actas 3, 131–163 Buenos Aires.

Charrier, R., Pinto, L., Rodríguez, M.P., 2007. Tectonostratigraphic evolution of the Andean Orogen in Chile. In: Moreno T. and Gibbons W. (Eds), The Geology of Chile. The Geological Society, London, 21-114.

Charrier, R., Ramos, V.A., Tapia, F., Sagripanti, L., 2014. Tectono-stratigraphic evolution of the Andean Orogen between 31 and 37°S (Chile and Western Argentina). In: Sepúlveda, S.A., Giambiagi, L.B., Moreiras, S.M., Pinto, L., Tunik, M., Hoke, G.D., Farías, M. (Eds.), Geodynamic Processes in the Andes of Central Chile and Argentina. Geological Society, London, Special Publications, vol. 399. pp. 13–61.

Cingolani, C.A., Llambías, E.J., Basei, M.A.S., Varela, R,. Chemale, F. Jr., Abre, P., 2005. Grenvillian and Famatinina-age igneous events in the San Rafael Block, Mendoza Province, Argentina: geochemical and isotopic constraints. In: Pankhurst RJ, Veiga GD (eds) Gondwana 12. Academia Nacional de Ciencias, Mendoza, p 103.

Corbella, H., Novas, F.E., Apesteguía, S., Leanza, H.A., 2004. First fission track-age for the dinosaur-bearing Neuquén Group (Upper Cretaceous) Neuquén basin, Argentina. Revista Museo Argentino de Ciencias Naturales 6 (2), 1–6 (n.s).

Critelli, S., Ingersoll, R. V., 1995. Interpretation of neovolcanic versus palaeovolcanic sand grains: an example from Miocene deep-marine sandstone of the Topanga Group (Southern California). Sedimentology 42: 783–804.

Di Giulio, A., Ronchi, A., Sanfilippo, A., Balgord, E., Carrapa, B., Ramos, V.A., 2016. Cretaceous evolution of the Andean margin between 36°S and 40°S latitude

through a multi-proxy provenance analysis of Neuquén Basin strata (Argentina). Basin Res. 29, 284–304.

Di Giulio, A., Ronchi, A., Sanfilippo, A., Tiepolo, M., Pimentel, M., Ramos, V.A., 2012. Detrital zircon provenance from the Neuquén Basin (south-central Andes): Cretaceous geodynamic evolution and sedimentary response in a retroarc-foreland basin. Geology 40, 559–562.

Dickinson, W. R., Gehrels G. E., 2009. Use of U-Pb ages of detrital zircons to infer maximum depositional ages of strata: A test against a Colorado Plateau database, Earth Planet. Sci. Lett., 288(1–2), 115–125, doi:10.1016/j.epsl.2009.09.013.

Dickinson, W.R., Beard, L.S., Brakenridge, G.R.,Erjavec, J.L., Ferguson, R.C. Inman, K.F.,Knepp, R.A. Lindberg, F.A., Ryberg, P.T., 1983. Provenance of North American Phanerozoicsandstones in relation to tectonic setting:Geological Society of America, Bulletin94: 222-235.

Dickson, J. A. D., 1965. A modified staining technique for carbonates in thin section. Nature 205 (4971), 587-587.

Dingus, L., Clarke, J., Scott, G.R., Swisher, C.C., Chiappe, L.M., Coria, R.A., 2000. Stratigraphy and magnetostratigraphic/faunal constrains for the age of sauropod embryo-bearing rocks in the Neuquén Group (Late Cretaceous, Neuquén province, Argentina). American Museum Novitates 3290: 1-11.

Fennell, L., Folguera, A., Naipauer, M., Gianni, G., Rojas Vera, E., Bottesi, G., Ramos, V.A., 2017a. Cretaceous deformation of the southern Central Andes: synorogenic growth strata in the Neuquén Group (35°30′–37°S). Basin Research. 29, 51–72.

Fennell, L., Naipauer, M., Folguera, A., 2017b. El movimiento Intersenoniano de Pablo Groeber en el norte de Neuquén y Sur de Mendoza: bases de la primera orogenia andina. Revista de la Asociación Geológica Argentina; Año: 2017 vol. 74 p. 59 - 73.

Folguera, A., Bottesi, G., Duddy, I., Martín-González, F., Orts, D., Sagripanti, L., Rojas Vera, E.A., Ramos, V.A., 2015. Exhumation of the Neuquén Basin in the southern Central Andes (Malargüe fold and thrust belt) from field data and low-

temperature thermochronology. Journal of South American Earth Sciences 64: 381-398.

Folk, R.L., Andrews, P.B; Lewis, D.W., 1970. Detrital sedimentary rock classification and nomenclature for use in New Zeland. New Zeland Journal of Geology and Geophysics 13: 937-968.

Garrido, A.C., 2010. Estratigrafía del Grupo Neuquén, Cretácico Superior de la Cuenca Neuquina (República Argentina): Nueva propuesta de ordenamiento litoestratigráfico. Revista del Museo Argentino de Ciencias Naturales, Nueva Serie, 12 (2).

Gehrels, G. E., V. Valencia, and A. Pullen., 2006. Detrital zircon geochronology by Laser– Ablation Multicollector ICPMS at the Arizona LaserChron Center, in Geochronology: Emerging Opportunities, Paleontological Society Short Course, October 21, 2006, Philadelphia, PA,edited by T. Olszewski and W. Huff, Paleontol. Soc. Pap., 12, 1–10.

Gehrels, G. E., V. Valencia, J. Ruiz., 2008. Enhanced precision, accuracy, efficiency, and spatial resolution of U□Pb ages by laser ablation– multicollector inductively coupled plasma–mass spectrometry, Geochem. Geophys. Geosyst., 9, Q03017, doi:10.1029/2007GC001805.

Gianni, G. M., Dávila, F. M., Echaurren, A., Fennell, L., Tobal, J., Navarrete, C., Quezada, P., Folguera, A., Giménez, M., 2018. A geodynamic model linking Cretaceous orogeny, arc migration, foreland dynamic subsidence and marine ingression in southern South America. Earth-Science Reviews Vol. 185: 437-462

Gómez R., Tunik M., Casadío S., 2016a. Análisis de facies del Grupo Neuquén, Cretácico Superior, en el área Vega Grande, Mendoza, Argentina. Congreso. VII Congreso Latinoamericano de Sedimentología, CLS- y la XV Reunión Argentina de Sedimentología. Santa Rosa, La Pampa.

Gómez R., Tunik M., Casadío S., 2016b. Icnología del Grupo Neuquén (Cretácico Superior), Vega Grande, Mendoza: caracterización e importancia paleoambiental. Congreso. 11° Congreso de la Asociación Paleontológica Argentina. General Roca, Río Negro.

Groeber, P. 1946. Observaciones geológicas a lo largo del meridiano 70°. 1, Hoja Chos Malal. Revista de la Sociedad Geológica Argentina 1(3): 117-208. Reimpreso

en Asociación Geológica Argentina, Serie C, Reimpresiones 1: 1-174 (1980), Buenos Aires.

Howell, J.A., Schwarz, E., Spalletti, L., Veiga, G.D., 2005. The Neuquén Basin: an overview. In: Veiga, G., et al. (Ed.), The Neuquén Basin: a Case Study in Sequence Stratigraphy and Basin Dynamics: The Geological Society, Special Publication, 252, pp. 1–14.

Ingersoll, R. V., Fullard, T. F., Ford, R. L., Grimm, J. P., Pickle, J. D., Sares, S. W., 1984. The effect of grain size on detrital modes; a test of the Gazzi–Dickinson point-counting method. Journal of Sedimentary Research 54, 103–116.

Kay, S.M., Ramos, V.A., Mpodozis, C., Sruoga, P., 1989. Late Paleozoic to Jurassic silicic magmatism at the Gondwanaland margin: analogy to the Middle Proterozoic in North America? Geology 17, 324–328.

Kleiman, L.E., Japas, M.S., 2009. The Choiyoi volcanic province at 34°S-36°S (San Rafael, Mendoza, Argentina): Implications for the Late Palaeozoic evolution of the southwestern margin of Gondwana. Tectonophysics, 473(3-4), 283-299. http://dx.doi.org/10.1016/j.tecto.2009.02.046

Kozlowski, E., Manceda, R., Ramos, V.A., 1993. Estructura. In Geología y Recursos Naturales de Mendoza (Ramos, V.A.; editor). Congreso Geológico Argentino, No. 12 y Congreso de Exploración de Hidrocarburos, No. 2, Relatorio: 235-256. Buenos Aires.

Leanza, H.A., 2003. Las sedimentitas huitrinianas y rayosianas (Cretácico inferior) en el ámbito central y meridional de la cuenca Neuquina, Argentina. Servicio Geológico Minero Argentino, Serv. Geol. Min. Argentino, Contr. Tec-Geol., 2, 1–31.

Leanza, H.A., 2009. Las principales discordancias del Mesozoico de la Cuenca Neuquina según observaciones de superficie. Rev. Mus. Argent. Cienc. Nat. Nueva Ser., 11(2), 145–184.

Leanza, H.A., Apesteguía, S., Novas, F.E., de la Fuente, M.S., 2004. Cretaceous terrestrial beds from the Neuquén Basin (Argentina) and their tetrapod assemblages. Cretac. Res., 25, 61–87.

Leanza, H.A., Hugo, C.A., 2001. Hoja Geológica 3969-I - Zapala, provincia del Neuquén. Instituto de Geología y Recursos Naturales. SEGEMAR. Boletín 275: 1- 128. Buenos Aires.

ACCEPTED MANUSCRIPT

Legarreta, L., Gulisano, C.A., 1989. Análisis estratigráfico secuencial de la Cuenca Neuquina (Triásico superior - Terciario inferior). En: G. Chebli & L. Spalletti (Eds.), Cuencas Sedimentarias Argentinas. X° Congreso Geológico Argentino. Serie Correlación Geológica 6: 221-243. Buenos Aires.

Legarreta, L., Uliana, M.A., 1998. Anatomy of hinterland depositional sequences: Upper Cretaceous fluvial strata, Neuquén basin, west-central Argentina. In: Shanley, K.W., McCabe, P.J. (Eds.), Relative role of Eustasy, Climate, and Tectonism in Continental Rocks: SEPM Special Publication, 59, pp. 83–92.

Lothari, L., Gómez, R., Tunik, M., Toffani, M., 2018. Análisis sedimentológico y petrográfico de las Formaciones Rayoso y Diamante en el norte de la cuenca Neuquina, sur de Mendoza. 10° Congreso de Exploración y Desarrollo de Hidrocarburos. Noviembre, 2018. Mendoza, Argentina. Libro de actas, Programa de Estudiantes, 91-108.

Ludwig, K.R., 2012. User's manual for Isoplot 3.75. A geochronological toolkit for Microsoft Excel. Berkeley Geochronology Center Special Publication No. 5, 75 pp.

Ludwing, K.R., Mundil, R., 2002. Extracting reliable U-Pb ages and errors from complex populations of zircons from Phanerozoic tuffs: Geochimica et Cosmochimica Acta, v. 66, p.463.

Mackaman-Lofland, C., Horton, B..K, Fuentes, F., Kurt N.C., Stockli, D.F., 2019. Mesozoic to Cenozoic retroarc basin evolution during changes in tectonic regime, southern Central Andes (31–33°S): Insights from zircon U-Pb geochronology. Journal of South American Earth Sciences 89, 299-318.

Manceda, R., Figueroa, D., 1995. Inversion of the Mesozoic Neuquén rift in the Malargüe fold-thrust belt, Mendoza, Argentina. In Petroleum Basins of South America (Tankard, A.J.; Suárez, R.; Welsink, H.J.; editors). American Association of Petroleum Geology, Memoir 62: 369-382.

Mescua, J., Giambiagi, L.B., Ramos, V.A., 2013. Late Cretaceous Uplift in the Malargüe fold-and-thrust belt (35°S), southern Central Andes of Argentina and Chile. Andean Geol. 40, 102–116.

ACCEPTED MANUSCRIPT

Miall, A.D., 1996. The Geology of Fluvial Deposits, Vol. 575. Springer, Berlin.

Mosquera, A., Ramos, V., 2006. Intraplate deformation in the Neuquen embayement. In: Evolution of an Andean Margin: A Tectonic and Magmatic View From the Andes to the Neuquén Basin (35°-39° S lat.) (Ed. by S.M. Kay & V. Ramos) Geol. Soc. Am., Spec. Paper, 407, 97–123.

Muñoz, M., Tapia, F., Persico, M., Benoit, M., Charrier, R., Farías, M., Rojas, A., 2018. Extensional tectonics during Late Cretaceous evolution of the southern Central Andes: evidence from the Chilean main range at ~35°S. Tectonophysics. https://doi.org/10. 1016/j.tecto.2018.06.009.

Naipauer, M., Tunik, M., Marques, J. C., Rojas Vera, E. A., Vujovich, G. I., Pimentel, M. M., Ramos, V. A., 2015. U–Pb detrital zircon ages of Upper Jurassic continental successions: implications for the provenance and absolute age of the Jurassic–Cretaceous boundary in the Neuquén Basin. Geological Society, London, Special Publications, 399(1), 131–154. doi:10.1144/sp399.1

Orts, D.L., Folguera, A., Giménez, M., Ramos, V.A., 2012. Variable structural controls through time in the Southern Central Andes (~36ºS). Andean Geology 39(2): 220-241.

Ponce, J.J.; Zavala, C., Marteau, M., Drittanti D., 2002. Análisis estratigráfico y modelo deposicional para la Formación Rayoso (Cretácico Inferior) en la Cuenca Neuquina, provincia del Neuquén. Congreso Geológico Argentino, No. 15, Actas 1: 716-721. El Calafate.

Potter, P. E., 1994. Modern sands of South America: composition, provenance and global significance. Geologische Rundschau 83: 212-232.

Ramos VA., Basei M., 1997. The basement of Chilenia: an exotic continental terrane to Gondwana during the Early Paleozoic. In: Bradshaw JD, Weaver SD (eds) Terrane Dynamics-97, International conference on terrane geology (Christchurch), conference abstracts, pp 140–143.

Ramos, V.A., 1981. Descripción geológica de la Hoja 33c Los Chihuidos Norte, Provincia del Neuquén. Servicio Geológico Nacional, Boletín 182, 1–103 Buenos Aires.

Ramos, V.A., 1999. In: Caminos, R. (Ed.), Rasgos estructurales del territorio argentino. Geología Argentina. vol. 29(24). Instituto de Geología y recursos Minerales, Anales, pp. 715–784.

Ramos, V.A., 2010. The Grenville-age basement of the Andes. Journal of South American Earth Sciences 29 (1), 77–91.

Rojas Vera, E.A., Sellés, D., Folguera, A., Gímenez, M., Ruíz, F., Orts, D., Zamora Valcarce, G., Martínez, P., Bechis, F., Ramos, V.A., 2014. The origin of the Loncopué Trough in the retroarc of the Southern Central Andes from field, geophysical and geochemical data. Tectonophysics 637, 1–19.

Rossel, P., Oliveros, V., Mescua, J., Tapia, F., Ducea, M.N., Calderón, S., Charrier, R., Hoffman, D., 2014. El volcanismo Jurásico superior de la Formación Río Damas-Tordillo (33°-35,5°S): antecedentes su sobre petrogénesis, cronología, proveniencia e implicancias tectónicas. Andean Geology 41, 529–557. https://doi.org/10.5027/andgeoV41n3-a03.

Scasso, R. A., Limarino, C.O., 1997. Petrología y Diagénesis de Rocas Clásticas. Asociación Argentina de Sedimentología. Publicación Especial 1: 258 pp. Buenos Aires.

Silvestro, J., Zubiri, M., 2008 Convergencia oblicua: modelo estructural alternativo para la dorsal Neuquina (39ºS), Neuquén. Revista Asociación Geológica Argentina 63: 49-64.

Thomas W.A., Tucker R.D., Astini R.A., Denison R.E., 2012. Ages of pre-rift basement and synrift rocks along the conjugate rift and transform margins of the Argentine Precordillera and Laurentia. Geosphere 8(6):1366–1383.

Tunik, M. A., 2001. Análisis sedimentológico y tectónico de la primera ingresión atlántica en la Alta Cordillera de Mendoza. Tesis doctoral (inédito). Facultad de Ciencias Exactas y Naturales, Universidad de Buenos Aires: 257 p.

Tunik, M., Folguera, A., Naipauer, M., Pimentel, M., Ramos, V., 2010. Early uplift and orogenic deformation in the Neuquén Basin: constraints on the Andean uplift from U–Pb and Hf isotopic data of detrital zircons. Tectonophysics 489, 258 273.

Turienzo, M.M. 2009. La estructura de la faja corrida y plegada de Malargüe en la zona del río Diamante (34º30'-34º50' L.S.) y su relación con la Cordillera Frontal,

provincia de Mendoza. Revista de la Asociación Geológica Argentina 65 (1): 123-139.

Uliana, M.A., Dellapé, D.A., 1981. Estratigrafía y evolución paleoambiental de la sucesión maestrichtiano-eoterciaria del engolfamiento neuquino (Patagonia septentrional). 8° Congreso Geológico Argentino (San Luis), Actas3: 673-711.

Uliana, M.A., Dellapé, D.A., Pando, G.A., 1975. Distribución y génesis de las sedimentitas rayosianas (Cretácico inferior de las provincias de Neuquén y Mendoza). 2° Congreso Ibero-Americano de Geología Económica, Actas 1, 151–176 Buenos Aires.

Vergani, G., Tankard, A.J., Belotti, H.J., Welsnik, H.J., 1995. Tectonic evolution and paleogeography of the Neuquén Basin, Argentina. In: Petroleum Basins of South America, AAPG Memoir, 62, pp. 383–402. https://doi.org/10.1306/7834F6E1-1721- 11D7-8645000102C1865D.

Vergara, M., Levi, B., Nystrom, J., Cancino, A., 1995. Jurassic and Early Cretaceous island arc volcanism, extension, and subsidence in the Coast Range of central Chile. Geological Society of America Bulletin 107: 1427-1440.

Zamora Valcarce, G., Zapata, T., Ramos, V.A., Rodriguez Monreal, F., Bernardo, L., 2009. Evolución tectónica del frente andino en Neuquén. Revista de la Asociación Geológica Argentina. 65, 192-203.

Zavala, C., Ponce, J., Drittanti, D., Arcuri, M., Freije, H., Asensio, M., 2006. Ancient Lacustrine Hyperpycnites: a Depositional Model from a Case Study in the Rayoso Formation (Cretaceous) of west-Central Argentina. Journal of Sedimentary Research 76: 41-59.

Zavala, C., Ponce, J., Marteau, M., 2001. Origin, Sequence Stratigraphy and Hydrocarbon Potential of the Rayoso Formation (Aptian-Albian) in the Central Neuquén Basin (Argentina). American Association of Petroleum Geologists Hedberg Conference «New Technologies and New Play Concepts in Latin America», Abstracts: 35-36. Mendoza.

Epigraphs

Figures

Figure 1. Map showing the location of the Neuquén Basin and the study area (modified from Tunik et al., 2010; Balgord and Carrapa, 2016) and the position of the Late Cretaceous thrust front (Mescua et al., 2013; Fennell et al., 2017a, b).

Figure 2. Local geological map showing the main units and the position of stratigraphic sections, Vega Grande and Vega de los Patos (modified of Lothari et al., 2018).

Figure 3. Measured stratigraphic section from Vega Grande area.

Figure 4. Measured stratigraphic section from Vega de los Patos area.

Figure 5. Photographs of outcrops; a) the transitional contact between Diamante and Saldeño formations in Vega Grande oil field., b) the transitional contact between Huitrín and Rayoso formations (Bajada del Agrio Group)., c) laminated-mudstones with interbedded gypsum (yellow arrows) from the Rayoso Formation., d) massive sandstone from de base of the Diamante Formation.

Figure 6. Photographs of outcrops; a) Vega de los Patos anticline showing the position and contact between units., b) Diamante Formation on Vega Grande area, c) reworked tuff deposit from the top of Vega Grande section (VG24-16 sample), d) conglomerate from Vega de los Patos section, composed almost exclusively of carbonate fragments (CC).

Figure 7. a) VG1 sample. Photomicrographs of framework composition: monocrystalline quartz (Qm), alkaline feldspar (Fk), plagioclase (Fpl), granular (Lpg) and seriate (Lps) paleovolcanic lithic fragments. Analcime as a type of zeolitic cement (Cc). Photomicrographs on NP and NX. Scale: 100 microns. b) VG4 sample. Photomicrographs of framework composition: monocrystalline quartz (Qm), alkaline feldspar (Fk), plagioclase (Fpl) and pyroclastic paleovolcanic lithic fragment (Lp), with altered vitreous shard. Photomicrographs on NX. Scale: 100 microns c) VG16-16 sample. Photomicrographs of framework composition: high percentage of limestone lithic fragments (Lc). Scale: 60 microns. d) VLP02 sample. Photomicrographs of framework composition it composed of monocrystalline quartz (Qm), alkaline feldspar (Fk), metamorphic lithic (Lm), analcime - zeolitic cement (Cc) and porosity (P).

ACCEPTED MANUSCRIPT

Photomicrographs on NX. Scale: 100 microns. e) VLP06 sample. Photomicrographs of framework composition it composed of monocrystalline quartz (Qm), alkaline feldspar (Fk), granular (Lpg) and serial (Lps) paleovolcanic lithic fragments, other lithic (Lo) and porosity (P). Photomicrographs on NX. Scale: 100 microns. f) VLP09 sample. Photomicrographs of framework composition it composed of monocrystalline quartz (Qm), alkaline feldspar (Fk), granular (Lpg) and serial (Lps) paleovolcanic lithic fragments, calcite cement (Cca) and metamorphic lithic (Lm). Photomicrographs on NP. Scale: 100 microns. NP: parallel nicols, NX: crossed nicols.

Figure 8. a) Sandstone classification QFL plot according to Folk *et al.* (1970) of the analyzed samples; b) QFL and QmFLt plots of sandstones from Diamante Formation to discriminate provenance areas. On the left, QFL diagram from Dickinson et al. (1983). On the right, QmFLt from Dickinson et al. (1983). Q: total quartz, F: total feldspar, L: total lithic fragments, Qm: monocrystalline quartz, Lt: total lithic fragments plus polycrystalline quartz.

Figure 9. a) Frequency histograms, relative probability plots, and concordia plots of U–Pb ages from analysed zircons (Vega Grande sample-VG24-16; Vega de los Patos sample-VLP001-17) showing the important source areas (highlighted in different colours). The number of grains in each sample is denoted with n = x below sample name.

Figure 10. The weighted mean ages calculated with the youngest zircon grains (1r errors overlap) from the samples: a) VG24-16 (Vega Grande); b) VLP001-17 (Vega de los Patos). This age overlaps the TuffZirc age (with uncertainties) for the youngest cluster of coherent grain ages.

Tables

Table 1. Populations of ages of both samples: A: Jurassic and Cretaceous; B: Permian-Triassic; C: Ordovician-Devonian; D: Neoproterozoic-Cambrian; E: Meso-NeoProterozoic; F: Mesoproterozoic; G: Paleoproterozoic; H: Neoarchean.

Appendix

1) Clast counting

		SAMPLES-VEGA DE LOS PATOS (% in weight)								SAMPLES-VEGA GRANDE (% in weight)									
		VLP01	VLP02	VLP03	VLP04	VLP05	VLP06	VLP07a	VLP09	VG1	VG2	VG3	VG4	VG5	VG8	VG9	VG13	VG16	VG17
QUARTZ (Q)	Qf	13.5	13.25	14.75	8.75	16.5	12.25	17.25	14.5	24	9.25	27.5	30.75	26.5	23	31	29.5	11	27.75
	Qo	3.75	5.25	4.25	3.75	4.5	5.5	5	5.25	6.5	0.25	1.5	3.75	5	9	1	0.75	3	5.5
	Qv	3.5	3	2.5	10.5	5	8.75	4.75	6.25	2.75	3.75	1.75	5.25	1	1.5	2.5	3.25	0	1
	Qp	2.5	2.5	5.25	7	3.25	6.5	3.5	10.25	4.25	9	7	5.5	5	3.25	4	4	1.25	8.5
FELDSPAR (F= K+P)	Fk	5.75	9	6.75	5.75	9	9.5	9.25	8.5	8.75	2	2.25	6	7	3.75	5.5	5.5	4.75	8.75
	Fpl	9	8.25	5.5	1.25	3	2.75	3.5	3	10.5	2	3.75	3	6.5	8	4.5	5	3.5	2.5
	Fkp	0	0	0	0.75	0	0.75	0	0.25	0	2.25	0.75	0.25	0	0	0.25	0	1	1.5
	FPp	0	1.5	1	3.5	0.75	0.5	1.25	3.25	0	1.5	0.5	0.75	0	1	0	0.25	1.75	0.5
	Fc	0	0	0	0	0	0	0	0	0	0	0	0	0	0	0	0	2.25	0
LITHICS (L)	Lpg	10.75	13	7.5	10.75	13.25	16	15.75	18.75	13.5	9.75	13	15.75	10.75	7.25	13.75	10.25	4.25	7.5
	Lps	5	5	3.75	9	6.25	5.75	6	3.75	3.75	3.75	0.25	0.75	4.25	13.5	8	4.75	0.5	2.25
	Lpp	3.25	3.5	6.75	3.75	4.75	1.5	3.75	1.5	9.25	8.5	0	0.25	8.75	10	0	2.5	0	0.25
	Lpl	4.5	3.75	1.25	0.75	0.25	0	0	0.5	0	0	0.5	0	0	0	0	0	0.25	0
	Lc	0	0	0	0	0	0	0	0	0	0	0	0	0	0	0	0	34.25	0
	Ls	2.25	2.5	0.75	2.25	1.75	0	0.25	2.75	0.75	3	2.75	3	0.75	0	0.75	1.75	4.75	3.25
	Lp	1	0.75	0.5	3.5	1.5	2.25	1	1.25	0	0	0	0	0	0.5	0.25	0	0	0
	Lm	1.5	0.5	1.5	2.25	4	1	3	0.25	0.75	1	3.25	1.5	1.75	2	1	0.5	0	0
	La	3.5	2.75	5.25	5.25	2.25	1.75	2	2	8	11	8	7	9	4.75	4	3.25	5.25	8.75
CEMENTS	Cc	6.5	7.75	8	2	2.5	3.75	2.25	1.75	6.25	0.5	0	0	2	1.75	8	3.25	0.5	0
	Ca	2	0.25	0	1	2.75	2	2	1.5	0	1.25	4	1.75	2.25	0.75	0.5	0.25	0.25	0.75
	Cf	8.75	6.75	12	1.5	1.25	6.25	6	2	0	3.25	2.75	1.5	0	0	4.75	2.5	3.75	1.25
	Ccar	0	0.75	0.25	11.75	9.25	6	0	5	0.5	24.75	3.75	2.5	5.75	4.5	2.25	10.75	15.25	2.25
	Co	1	0	0	0	1	0	2.5	0	0	0.5	0	1.75	0		1	0.5	0	0
OTHER	M	0.25	0	0	0	0	0.25	2.5	0	0.25	0	1	0.25	0.25	0	0	0.25	0	0.25
	Op	4.25	6.75	6	0.75	1.25	2.25	2.5	0.75	0	1	0.25	1.75	1.25	0.75	0.75	0.75	0.25	2.5
	Om	0	0	0	0	0	0	0	0	0	0	0	0	0.5	0	0	0	0	0
	O	7.5	3.25	6.5	4.25	6	4.75	6	7	0.25	1.75	15.5	7	1.75	4.75	6.25	10.5	2.25	15
		100	100	100	100	100	100	100	100	100	100	100	100	100	100	100	100	100	100

ACCEPTED MANUSCRIPT

Abbreviations used in point-count data table and equations for values (*Clast counting*)

Qf: non-undulatory monocrystalline quartz

Qo: undulatory monocrystalline quartz;

Qv: quartz on volcanic rock grain;

Qp: polycrystalline quartz;

Fk: alkaline feldspar;

Fpl: plagioclase feldspar;

Fkp: alkaline feldspar on paleovolcanic lithic grain;

Fc: feldspar replaced by calcite;

FPp: plagioclase on paleovolcanic lithic grain;

Lpg: granular texture on paleovolcanic lithic grain;

Lps: serial texture on paleovolcanic lithic grain;

Lpp: pyroclastic lithic grain;

Lpl: lathwork texture on paleovolcanic texture;

Lpm: microlitic texture on paleovolcanic lithic grain;

Lc: carbonate lithic grain;

Ls: another sedimentary lithic grain (generally siltstone);

Lp: plutonic lithic grain;

Lm: metamorphic lithic grain;

La: altered and undetermined lithic grain;

Cc: zeolitic cement;

Ca: argillaceous cement;

Cf: iron cement;

Ccar: calcareous cement;

Co: other cements; M-micas;

Op: opaques;

Om: other minerals;

O/P: porosity. Recalculated values:

ACCEPTED MANUSCRIPT

2) U/Pb detrital zircon geochronology

The analyses involve ablation of zircon with a Photon Machines Analyte G2 excimer laser using a spot diameter of 30 microns. All measurements are made in static mode, using Faraday detectors with 3x1011 ohm resistors for 238U, 232Th, 208Pb-206Pb, and discrete dynode ion counters for 204Pb and 202Hg. For each analysis, the errors in determining 206Pb/238U and 206Pb/204Pb result in a measurement error of ~1-2% (at 2- sigma level) in the 206Pb/238U age. The errors in measurement of 206Pb/207Pb and 206Pb/204Pb also result in ~1-2% (at 2-sigma level) uncertainty in age for grains that are >1.0 Ga, but are substantially larger for younger grains due to low intensity of the 207Pb signal. For most analyses, the cross-over in precision of 206Pb/238U and 206Pb/207Pb ages occurs at ~1.0 Ga.

Inter-element fractionation of Pb/U is generally ~5%, whereas apparent fractionation of Pb isotopes is generally <0.2%. In-run analysis of fragments of a large zircon crystal (generally every fifth measurement) with known age of 563.5 ± 3.2 Ma (2- sigma error) is used to correct for this fractionation. The uncertainty resulting from the calibration correction is generally 1-2% (2-sigma) for both 206Pb/207Pb and 206Pb/238U ages. Uncertainties shown in these tables are at the 1-sigma level, and include only measurement errors. Analyses that are >20% discordant (by comparison of 206Pb/238U and 206Pb/207Pb ages) or >5% reverse discordant are not considered further.

ACCEPTED MANUSCRIPT

ACCEPTED MANUSCRIPT

Table 1 A. U-Pb geochronologic analyses from sample VG24-16 (n=187)

						Isotope ratios					Apparent ages (Ma)								
Analysis	U	206Pb	U/Th	206Pb*	±	207Pb*	±	206Pb*	±	error	206Pb*	±	207Pb*	±	206Pb*	±	Best age	±	Conc
	(ppm)	204Pb		207Pb*	(%)	235U*	(%)	238U	(%)	corr.	238U*	(Ma)	235U	(Ma)	207Pb*	(Ma)	(Ma)	(Ma)	(%)
VG24-16	233	100454	1.5	20.4693	2.4	0.0856	3.1	0.0127	1.9	0.61	81.5	1.5	83.4	2.5	140.8	57.0	81.5	1.5	NA
VG24-16	286	1672	0.9	25.1637	3.9	0.0724	4.3	0.0132	1.8	0.43	84.6	1.5	70.9	2.9	NA	NA	84.6	1.5	NA
VG24-16	169	10059	2.3	21.7650	2.3	0.0850	2.9	0.0134	1.9	0.63	86.0	1.6	82.9	2.3	NA	NA	86.0	1.6	NA
VG24-16	365	3561	2.1	23.7023	5.0	0.0798	5.5	0.0137	2.3	0.42	87.9	2.0	78.0	4.1	NA	NA	87.9	2.0	NA
VG24-16	633	17096	1.0	21.5046	1.5	0.0907	2.3	0.0142	1.8	0.78	90.6	1.6	88.2	2.0	23.7	35.3	90.6	1.6	NA
VG24-16	146	1877	2.6	24.2294	3.4	0.0812	3.9	0.0143	1.9	0.49	91.3	1.7	79.2	3.0	NA	NA	91.3	1.7	NA
VG24-16	27	1362	1.9	7.5899	18.0	0.2609	18.2	0.0144	3.1	0.17	92.0	2.8	235.4	38.3	2121.5	317.6	92.0	2.8	NA
VG24-16	221	54275	1.1	17.7269	2.3	0.1369	2.8	0.0176	1.6	0.57	112.5	1.8	130.2	3.4	468.6	50.2	112.5	1.8	NA
VG24-16	191	23428	0.3	19.0376	1.6	0.2748	2.5	0.0380	1.9	0.76	240.2	4.5	246.5	5.5	308.5	37.1	240.2	4.5	NA
VG24-16	20	3486	1.7	19.8405	4.2	0.2681	5.1	0.0386	2.9	0.57	244.1	6.9	241.2	10.9	213.6	96.6	244.1	6.9	NA
VG24-16	74	5569	2.6	20.3395	2.2	0.2630	3.1	0.0388	2.2	0.70	245.5	5.3	237.1	6.6	155.7	52.2	245.5	5.3	NA
VG24-16	21	21485	2.5	20.3269	3.8	0.2677	4.5	0.0395	2.3	0.52	249.6	5.7	240.8	9.6	157.2	90.0	249.6	5.7	NA
VG24-16	32	2020	1.7	22.5361	6.6	0.2437	7.0	0.0399	2.3	0.32	251.9	5.6	221.5	13.8	NA	NA	251.9	5.6	NA
VG24-16	29	2018	1.4	21.7097	4.1	0.2553	4.6	0.0402	2.1	0.45	254.2	5.2	230.9	9.5	NA	NA	254.2	5.2	NA
VG24-16	336	26692	1.6	19.5335	1.5	0.2842	2.3	0.0403	1.8	0.76	254.6	4.5	254.0	5.3	249.6	34.8	254.6	4.5	NA
VG24-16	49	6698	0.8	19.3304	2.7	0.2879	3.4	0.0404	2.1	0.61	255.2	5.2	256.9	7.7	273.6	62.1	255.2	5.2	NA
VG24-16	73	5786	1.6	19.5637	3.0	0.2853	3.8	0.0405	2.3	0.62	255.9	5.8	254.9	8.5	246.0	68.7	255.9	5.8	NA
VG24-16	413	113869	1.5	19.5204	1.1	0.2869	2.3	0.0406	2.0	0.88	256.8	5.1	256.1	5.2	251.1	25.0	256.8	5.1	NA
VG24-16	184	24212	1.2	19.5695	1.9	0.2870	2.6	0.0407	1.7	0.68	257.5	4.4	256.2	5.8	245.3	43.2	257.5	4.4	NA
VG24-16	96	15354	1.0	19.7365	2.0	0.2847	2.6	0.0408	1.6	0.64	257.6	4.2	254.4	5.8	225.8	46.3	257.6	4.2	NA
VG24-16	389	163487	0.9	17.9622	2.5	0.3128	3.3	0.0408	2.2	0.66	257.6	5.5	276.4	8.0	439.3	55.3	257.6	5.5	NA
VG24-16	127	18735	1.9	19.4601	1.7	0.2896	2.6	0.0409	2.0	0.76	258.3	5.0	258.2	6.0	258.2	39.2	258.3	5.0	NA
VG24-16	42	11891	1.4	20.6367	3.2	0.2731	3.9	0.0409	2.2	0.57	258.4	5.6	245.2	8.4	121.6	74.6	258.4	5.6	NA
VG24-16	28	3261	1.9	19.7244	3.8	0.2859	4.4	0.0409	2.3	0.52	258.5	5.8	255.3	9.9	227.2	87.2	258.5	5.8	NA

ages for grains<1000 Ma based on 206Pb/238U values; ages for grains>1000 Ma based on 206Pb/207Pb

ACCEPTED MANUSCRIPT

Table 1 A. U-Pb geochronologic analyses from sample VG24-16 (cont) (n=187)

						Isotope ratios					Apparent ages (Ma)								
Analysis	U	206Pb	U/Th	206Pb*	±	207Pb*	±	206Pb*	±	error	206Pb*	±	207Pb*	±	206Pb*	±	Best age	±	Conc
	(ppm)	204Pb		207Pb*	(%)	235U*	(%)	238U	(%)	corr.	238U*	(Ma)	235U	(Ma)	207Pb*	(Ma)	(Ma)	(Ma)	(%)
VG24-16	69	13212	1.2	18.6296	2.2	0.3029	2.9	0.0409	1.9	0.65	258.7	4.8	268.7	6.8	357.5	49.8	258.7	4.8	NA
VG24-16	708	18981	1.7	19.5900	1.3	0.2882	2.3	0.0410	2.0	0.84	258.8	5.0	257.2	5.3	242.9	29.4	258.8	5.0	NA
VG24-16	150	10537	1.1	19.5902	1.7	0.2885	2.5	0.0410	1.8	0.73	259.1	4.6	257.4	5.6	242.9	38.6	259.1	4.6	NA
VG24-16	231	18599	2.2	19.6796	1.9	0.2874	2.9	0.0410	2.2	0.75	259.3	5.6	256.5	6.6	232.4	44.4	259.3	5.6	NA
VG24-16	54	4074	2.4	20.9040	3.4	0.2707	4.0	0.0411	2.1	0.52	259.4	5.3	243.2	8.7	91.2	81.7	259.4	5.3	NA
VG24-16	45	6756	1.2	20.8848	2.0	0.2711	3.1	0.0411	2.4	0.77	259.6	6.0	243.6	6.7	93.4	46.2	259.6	6.0	NA
VG24-16	105	14354	2.6	19.4654	1.9	0.2909	2.8	0.0411	2.1	0.74	259.6	5.4	259.3	6.5	257.6	43.8	259.6	5.4	NA
VG24-16	171	11765	1.9	19.8539	1.6	0.2855	2.3	0.0411	1.7	0.74	259.8	4.3	255.0	5.2	212.0	36.1	259.8	4.3	NA
VG24-16	177	21967	1.4	19.2773	1.9	0.2940	2.7	0.0411	1.9	0.70	259.8	4.8	261.7	6.2	279.9	44.3	259.8	4.8	NA
VG24-16	192	28459	1.4	19.2871	1.3	0.2942	1.9	0.0412	1.5	0.76	260.1	3.8	261.8	4.5	278.7	28.9	260.1	3.8	NA
VG24-16	85	4588	1.1	20.4621	2.2	0.2776	2.8	0.0412	1.7	0.62	260.3	4.4	248.7	6.2	141.7	51.6	260.3	4.4	NA
VG24-16	106	15415	1.1	19.4556	1.7	0.2921	2.3	0.0412	1.6	0.68	260.5	4.0	260.2	5.3	258.8	39.3	260.5	4.0	NA
VG24-16	120	28114	2.0	20.6143	2.0	0.2757	3.0	0.0412	2.2	0.75	260.5	5.6	247.3	6.5	124.2	46.3	260.5	5.6	NA
VG24-16	61	7188	1.3	20.7634	3.4	0.2738	3.9	0.0412	1.9	0.48	260.6	4.8	245.7	8.4	107.2	80.1	260.6	4.8	NA
VG24-16	45	19150	1.6	19.4967	2.6	0.2917	3.0	0.0413	1.5	0.50	260.7	3.8	259.9	6.8	253.9	59.4	260.7	3.8	NA
VG24-16	47	9461	1.7	19.9417	2.7	0.2854	3.4	0.0413	2.1	0.62	260.9	5.4	254.9	7.7	201.8	61.8	260.9	5.4	NA
VG24-16	106	9573	1.6	17.0417	2.4	0.3344	3.2	0.0413	2.1	0.65	261.2	5.3	292.9	8.1	555.2	52.9	261.2	5.3	NA
VG24-16	123	5243	1.2	20.5949	1.9	0.2779	2.9	0.0415	2.2	0.75	262.3	5.7	249.0	6.5	126.5	45.5	262.3	5.7	NA
VG24-16	113	5067	1.6	20.6041	2.2	0.2779	3.1	0.0415	2.1	0.69	262.4	5.5	249.0	6.8	125.4	52.7	262.4	5.5	NA
VG24-16	639	100495	2.7	18.8854	1.4	0.3033	2.1	0.0416	1.5	0.74	262.5	3.9	269.0	4.9	326.7	31.9	262.5	3.9	NA
VG24-16	146	8481	1.0	20.1138	1.9	0.2848	2.5	0.0416	1.7	0.67	262.6	4.3	254.5	5.6	181.8	43.2	262.6	4.3	NA
VG24-16	27	8735	1.7	20.6042	3.3	0.2782	3.6	0.0416	1.6	0.43	262.7	4.0	249.2	8.0	125.4	77.2	262.7	4.0	NA

ages for grains<1000 Ma based on 206Pb/238U values; ages for grains>1000 Ma based on 206Pb/207Pb

ACCEPTED MANUSCRIPT

Table 1 A. U-Pb geochronologic analyses from sample VG24-16 (cont) (n=187)

				Isotope ratios							Apparent ages (Ma)								
Analysis	**U**	**206Pb**	**U/Th**	**206Pb***	**±**	**207Pb***	**±**	**206Pb***	**±**	**error**	**206Pb***	**±**	**207Pb***	**±**	**206Pb***	**±**	**Best age**	**±**	**Conc**
	(ppm)	**204Pb**		**207Pb***	**(%)**	**235U***	**(%)**	**238U**	**(%)**	**corr.**	**238U***	**(Ma)**	**235U**	**(Ma)**	**207Pb***	**(Ma)**	**(Ma)**	**(Ma)**	**(%)**
VG24-16	515	43539	1.5	19.8098	1.2	0.2894	2.3	0.0416	1.9	0.85	262.7	5.0	258.1	5.2	217.2	27.8	262.7	5.0	NA
VG24-16	383	24499	1.1	19.5924	1.7	0.2929	2.7	0.0416	2.1	0.79	263.0	5.5	260.8	6.3	242.6	38.6	263.0	5.5	NA
VG24-16	228	18508	1.5	19.7464	1.4	0.2908	2.5	0.0417	2.1	0.84	263.1	5.4	259.2	5.7	224.6	31.5	263.1	5.4	NA
VG24-16	70	5854	1.8	19.9589	3.1	0.2878	3.8	0.0417	2.3	0.61	263.2	6.0	256.8	8.7	199.8	71.0	263.2	6.0	NA
VG24-16	169	13349	1.2	19.8472	1.6	0.2897	2.5	0.0417	1.9	0.77	263.5	4.9	258.3	5.7	212.8	36.8	263.5	4.9	NA
VG24-16	123	6676	1.2	19.6843	1.6	0.2923	2.4	0.0417	1.8	0.76	263.6	4.8	260.3	5.6	231.8	37.0	263.6	4.8	NA
VG24-16	86	7081	1.9	20.2106	1.9	0.2848	2.6	0.0418	1.8	0.67	263.7	4.6	254.4	5.9	170.6	45.2	263.7	4.6	NA
VG24-16	399	141404	1.3	19.1554	1.3	0.3010	2.3	0.0418	1.9	0.82	264.2	4.9	267.2	5.3	294.4	29.4	264.2	4.9	NA
VG24-16	530	256022	1.8	17.9581	1.4	0.3218	2.4	0.0419	2.0	0.82	264.8	5.1	283.3	6.0	439.8	31.1	264.8	5.1	NA
VG24-16	178	48490	2.4	19.7481	1.5	0.2929	2.4	0.0420	1.8	0.77	265.1	4.8	260.9	5.5	224.3	35.6	265.1	4.8	NA
VG24-16	308	41869	1.7	19.5742	1.1	0.2956	2.0	0.0420	1.7	0.84	265.2	4.3	263.0	4.6	244.8	24.7	265.2	4.3	NA
VG24-16	638	38352	2.1	19.5664	1.1	0.2961	2.0	0.0420	1.6	0.81	265.4	4.2	263.3	4.6	245.7	26.3	265.4	4.2	NA
VG24-16	263	29515	2.3	19.9275	1.5	0.2909	2.4	0.0421	1.8	0.78	265.6	4.8	259.3	5.4	203.4	34.7	265.6	4.8	NA
VG24-16	22	905	1.1	25.7808	8.6	0.2249	8.9	0.0421	2.1	0.24	265.6	5.5	205.9	16.6	NA	NA	265.6	5.5	NA
VG24-16	152	13691	6.0	19.9303	1.6	0.2909	2.2	0.0421	1.6	0.71	265.6	4.2	259.3	5.1	203.1	36.3	265.6	4.2	NA
VG24-16	260	7536	1.2	20.3585	1.6	0.2848	2.9	0.0421	2.4	0.84	265.7	6.3	254.5	6.5	153.5	36.8	265.7	6.3	NA
VG24-16	429	185676	2.5	17.0380	2.0	0.3405	2.7	0.0421	1.8	0.67	265.8	4.6	297.6	6.9	555.7	43.3	265.8	4.6	NA
VG24-16	29	2130	1.9	21.4402	3.8	0.2709	4.4	0.0421	2.1	0.48	266.1	5.5	243.4	9.5	30.9	92.3	266.1	5.5	NA
VG24-16	260	17684	2.6	19.6767	1.5	0.2954	2.1	0.0422	1.5	0.71	266.3	4.0	262.8	5.0	232.7	34.8	266.3	4.0	NA
VG24-16	237	13273	2.2	20.4617	1.6	0.2845	2.2	0.0422	1.5	0.68	266.7	3.9	254.2	4.9	141.7	37.8	266.7	3.9	NA
VG24-16	419	31685	2.1	19.7083	1.5	0.2957	2.4	0.0423	1.9	0.79	267.0	5.0	263.1	5.5	229.0	33.5	267.0	5.0	NA
VG24-16	327	24815	1.9	19.7761	1.4	0.2948	2.6	0.0423	2.2	0.85	267.1	5.7	262.3	5.9	221.1	31.5	267.1	5.7	NA

ages for grains<1000 Ma based on 206Pb/238U values; ages for grains>1000 Ma based on 206Pb/207Pb

ACCEPTED MANUSCRIPT

Table 1 A. U-Pb geochronologic analyses from sample VG24-16 (cont) (n=187)

						Isotope ratios					Apparent ages (Ma)								
Analysis	U	206Pb	U/Th	206Pb*	±	207Pb*	±	206Pb*	±	error	206Pb*	±	207Pb*	±	206Pb*	±	Best age	±	Conc
	(ppm)	204Pb		207Pb*	(%)	235U*	(%)	238U	(%)	corr.	238U*	(Ma)	235U	(Ma)	207Pb*	(Ma)	(Ma)	(Ma)	(%)
VG24-16	149	13851	1.4	19.4574	1.3	0.3002	2.0	0.0424	1.5	0.75	267.6	3.9	266.5	4.7	258.5	30.0	267.6	3.9	NA
VG24-16	128	8167	1.1	19.9902	2.4	0.2929	3.0	0.0425	1.8	0.59	268.2	4.7	260.9	6.9	196.2	55.7	268.2	4.7	NA
VG24-16	839	359464	1.6	19.4409	1.1	0.3016	2.0	0.0425	1.6	0.82	268.6	4.3	267.7	4.7	260.5	26.1	268.6	4.3	NA
VG24-16	506	79798	1.8	19.2571	1.4	0.3053	2.4	0.0427	2.0	0.80	269.3	5.2	270.5	5.8	282.3	33.1	269.3	5.2	NA
VG24-16	353	19859	2.4	19.9441	1.2	0.2950	2.0	0.0427	1.7	0.82	269.5	4.4	262.5	4.7	201.5	27.1	269.5	4.4	NA
VG24-16	103	11633	1.6	20.2704	2.5	0.2903	3.3	0.0427	2.2	0.67	269.6	5.9	258.8	7.6	163.7	57.4	269.6	5.9	NA
VG24-16	468	43829	1.9	19.3417	1.2	0.3043	2.2	0.0427	1.8	0.84	269.6	4.8	269.8	5.2	272.2	27.4	269.6	4.8	NA
VG24-16	65	4331	1.1	20.9326	4.1	0.2816	4.6	0.0428	2.2	0.47	270.0	5.8	251.9	10.4	88.0	97.1	270.0	5.8	NA
VG24-16	224	14164	3.9	19.7446	1.4	0.2994	2.3	0.0429	1.9	0.81	270.7	5.0	265.9	5.4	224.8	31.2	270.7	5.0	NA
VG24-16	298	16875	2.2	19.6509	1.6	0.3013	2.5	0.0430	1.9	0.77	271.1	5.2	267.4	6.0	235.8	37.8	271.1	5.2	NA
VG24-16	27	5162	1.9	19.5978	4.0	0.3027	4.4	0.0430	1.8	0.42	271.7	4.9	268.5	10.3	242.0	91.5	271.7	4.9	NA
VG24-16	616	77705	1.7	19.4475	1.0	0.3052	1.8	0.0431	1.5	0.84	271.8	4.0	270.4	4.2	259.7	22.2	271.8	4.0	NA
VG24-16	232	56044	2.0	19.4640	1.6	0.3055	2.6	0.0431	2.0	0.79	272.3	5.4	270.7	6.1	257.8	36.5	272.3	5.4	NA
VG24-16	675	49426	1.8	19.0614	1.1	0.3120	1.9	0.0432	1.5	0.81	272.3	4.1	275.7	4.6	305.6	25.9	272.3	4.1	NA
VG24-16	503	23760	2.3	19.9067	1.2	0.2993	2.3	0.0432	1.9	0.86	272.9	5.2	265.9	5.3	205.9	27.3	272.9	5.2	NA
VG24-16	278	13595	1.7	19.6809	1.4	0.3031	2.0	0.0433	1.5	0.71	273.1	3.9	268.8	4.8	232.2	33.0	273.1	3.9	NA
VG24-16	210	154973	2.1	19.3845	1.9	0.3080	2.5	0.0433	1.7	0.66	273.4	4.4	272.6	6.0	267.2	43.6	273.4	4.4	NA
VG24-16	137	6813	2.0	14.1607	2.9	0.4217	3.5	0.0433	2.1	0.58	273.5	5.5	357.3	10.6	946.4	58.8	273.5	5.5	NA
VG24-16	98	23801	8.7	19.5414	1.7	0.3057	2.5	0.0433	1.8	0.74	273.5	4.9	270.8	5.9	248.6	38.6	273.5	4.9	NA
VG24-16	473	77914	3.5	19.2461	1.5	0.3111	2.2	0.0434	1.7	0.75	274.1	4.5	275.0	5.4	283.6	33.8	274.1	4.5	NA
VG24-16	480	157634	2.5	18.9182	1.1	0.3169	2.0	0.0435	1.7	0.83	274.5	4.5	279.5	4.9	322.8	25.5	274.5	4.5	NA
VG24-16	81	3107	1.1	10.2860	4.9	0.5843	5.5	0.0436	2.4	0.43	275.2	6.3	467.2	20.5	1571.4	92.4	275.2	6.3	NA

ages for grains<1000 Ma based on 206Pb/238U values; ages for grains>1000 Ma based on 206Pb/207Pb

ACCEPTED MANUSCRIPT

Table 1 A. U-Pb geochronologic analyses from sample VG24-16 (cont) (n=187)

						Isotope ratios					Apparent ages (Ma)								
Analysis	U	206Pb	U/Th	206Pb*	±	207Pb*	±	206Pb*	±	error	206Pb*	±	207Pb*	±	206Pb*	±	Best age	±	Conc
	(ppm)	204Pb		207Pb*	(%)	235U*	(%)	238U	(%)	corr.	238U*	(Ma)	235U	(Ma)	207Pb*	(Ma)	(Ma)	(Ma)	(%)
VG24-16	180	106254	0.9	19.4540	1.4	0.3091	2.0	0.0436	1.5	0.75	275.3	4.1	273.5	4.9	259.0	31.1	275.3	4.1	NA
VG24-16	34	2019	2.2	22.8393	4.0	0.2647	4.6	0.0439	2.2	0.48	276.7	6.0	238.4	9.7	NA	NA	276.7	6.0	NA
VG24-16	269	32604	1.1	19.2690	1.5	0.3139	2.4	0.0439	1.9	0.79	276.9	5.1	277.2	5.8	280.9	33.4	276.9	5.1	NA
VG24-16	425	58498	2.4	19.5552	1.3	0.3108	2.6	0.0441	2.3	0.87	278.2	6.3	274.8	6.3	247.0	29.6	278.2	6.3	NA
VG24-16	203	27728	2.0	18.9158	1.6	0.3244	2.6	0.0445	2.0	0.78	280.8	5.6	285.3	6.5	323.1	37.3	280.8	5.6	NA
VG24-16	343	164156	1.2	19.9201	1.3	0.3097	2.4	0.0448	2.0	0.84	282.3	5.6	273.9	5.7	204.3	29.8	282.3	5.6	NA
VG24-16	961	112473	1.0	18.3716	1.3	0.3429	2.3	0.0457	1.9	0.82	288.1	5.3	299.4	5.9	388.9	28.7	288.1	5.3	NA
VG24-16	200	21989	2.4	19.9375	1.3	0.3161	2.0	0.0457	1.6	0.78	288.2	4.5	278.9	5.0	202.2	29.9	288.2	4.5	NA
VG24-16	258	17272	2.8	19.1275	1.5	0.3450	2.1	0.0479	1.5	0.70	301.5	4.3	301.0	5.5	297.7	34.5	301.5	4.3	NA
VG24-16	440	75419	2.6	16.8001	2.0	0.4111	2.9	0.0501	2.1	0.72	315.2	6.5	349.7	8.6	586.3	43.7	315.2	6.5	NA
VG24-16	516	60171	1.6	18.2211	1.2	0.4622	2.2	0.0611	1.8	0.83	382.3	6.8	385.8	7.0	407.4	27.3	382.3	6.8	NA
VG24-16	1070	209089	1.4	18.0061	1.2	0.4713	1.9	0.0616	1.5	0.77	385.2	5.6	392.1	6.3	433.9	27.7	385.2	5.6	NA
VG24-16	292	7214	1.0	19.3267	1.0	0.4418	2.0	0.0620	1.8	0.88	387.5	6.8	371.5	6.3	274.0	21.8	387.5	6.8	NA
VG24-16	315	75206	1.5	17.7658	1.1	0.5034	2.3	0.0649	2.0	0.88	405.3	7.8	414.0	7.7	463.8	24.3	405.3	7.8	87.4
VG24-16	411	25687	77.6	17.8287	1.2	0.5662	2.2	0.0732	1.8	0.82	455.7	8.0	455.6	8.1	455.9	27.7	455.7	8.0	100.0
VG24-16	206	36081	0.6	17.7542	1.2	0.5723	2.3	0.0737	1.9	0.84	458.5	8.5	459.5	8.4	465.2	27.4	458.5	8.5	98.6
VG24-16	170	32819	1.6	17.6424	1.9	0.6022	2.6	0.0771	1.7	0.68	478.7	8.0	478.6	9.8	479.1	41.8	478.7	8.0	99.9
VG24-16	145	30940	1.9	17.3599	1.4	0.6697	2.4	0.0844	2.0	0.81	522.1	9.8	520.5	9.8	514.7	30.9	522.1	9.8	101.4
VG24-16	163	34897	3.0	17.2896	1.2	0.6727	2.2	0.0844	1.8	0.82	522.3	8.9	522.4	8.8	523.6	26.8	522.3	8.9	99.7
VG24-16	473	119354	9.0	17.2635	1.1	0.6765	2.1	0.0847	1.8	0.86	524.4	9.1	524.7	8.6	527.0	23.8	524.4	9.1	99.5
VG24-16	284	41230	1.6	16.9431	1.0	0.6968	1.8	0.0857	1.5	0.82	529.8	7.5	536.8	7.5	567.9	22.3	529.8	7.5	93.3
VG24-16	156	96230	3.4	16.4848	1.3	0.7267	2.7	0.0869	2.4	0.88	537.3	12.4	554.6	11.7	627.3	28.3	537.3	12.4	85.7

ages for grains<1000 Ma based on 206Pb/238U values; ages for grains>1000 Ma based on 206Pb/207Pb

ACCEPTED MANUSCRIPT

Table 1 A. U-Pb geochronologic analyses from sample VG24-16 (cont) (n=187)

						Isotope ratios					Apparent ages (Ma)								
Analysis	U	206Pb	U/Th	206Pb*	±	207Pb*	±	206Pb*	±	error	206Pb*	±	207Pb*	±	206Pb*	±	Best age	±	Conc
	(ppm)	204Pb		207Pb*	(%)	235U*	(%)	238U	(%)	corr.	238U*	(Ma)	235U	(Ma)	207Pb*	(Ma)	(Ma)	(Ma)	(%)
VG24-16	188	22847	1.1	17.0189	1.3	0.7222	2.1	0.0892	1.6	0.79	550.7	8.6	552.0	8.9	558.2	28.1	550.7	8.6	98.7
VG24-16	227	638939	1.1	16.8635	1.6	0.7504	2.5	0.0918	1.9	0.76	566.3	10.3	568.5	10.8	578.1	35.1	566.3	10.3	98.0
VG24-16	247	12656	4.9	16.7145	1.7	0.7756	2.7	0.0941	2.1	0.79	579.5	11.7	582.9	11.9	597.4	35.8	579.5	11.7	97.0
VG24-16	241	87257	4.9	15.7635	1.6	0.8296	2.7	0.0949	2.2	0.81	584.4	12.3	613.4	12.6	722.9	34.2	584.4	12.3	80.8
VG24-16	571	119924	145.9	16.7249	0.9	0.8050	1.9	0.0977	1.7	0.87	600.9	9.5	599.6	8.6	596.0	20.2	600.9	9.5	100.8
VG24-16	587	98417	3.8	16.1404	1.1	0.8393	3.0	0.0983	2.8	0.93	604.4	16.0	618.7	13.8	672.6	22.7	604.4	16.0	89.9
VG24-16	387	121497	4.4	16.7502	1.0	0.8177	2.1	0.0994	1.8	0.88	610.7	10.6	606.7	9.4	592.7	21.2	610.7	10.6	103.0
VG24-16	282	26145	2.9	16.2620	1.2	0.8455	2.1	0.0998	1.8	0.83	613.0	10.3	622.2	9.8	656.5	25.1	613.0	10.3	93.4
VG24-16	395	188640	4.8	16.7485	1.2	0.8318	2.5	0.1011	2.2	0.87	620.8	12.8	614.6	11.4	593.0	26.1	620.8	12.8	104.7
VG24-16	363	65809	3.1	16.4624	1.3	0.8611	2.3	0.1029	1.9	0.82	631.1	11.2	630.7	10.7	630.2	28.0	631.1	11.2	100.1
VG24-16	128	16034	0.7	16.3064	1.1	0.8715	2.3	0.1031	2.0	0.87	632.6	12.0	636.4	10.9	650.7	24.7	632.6	12.0	97.2
VG24-16	452	66797	2.4	16.6064	1.2	0.8683	2.1	0.1046	1.8	0.84	641.5	11.0	634.6	10.1	611.4	24.9	641.5	11.0	104.9
VG24-16	115	94180	1.3	16.3313	1.6	0.8929	2.4	0.1058	1.7	0.73	648.4	10.6	647.9	11.4	647.4	35.0	648.4	10.6	100.1
VG24-16	358	122453	15.1	16.3591	0.8	0.9059	1.9	0.1075	1.7	0.90	658.4	10.9	654.9	9.3	643.8	17.7	658.4	10.9	102.3
VG24-16	173	106034	3.3	15.5078	1.1	1.1551	1.9	0.1300	1.5	0.81	787.7	11.1	779.6	10.1	757.5	23.1	787.7	11.1	104.0
VG24-16	307	106944	1.6	15.2028	1.1	1.1859	2.0	0.1308	1.7	0.84	792.5	12.6	794.1	11.2	799.3	23.3	792.5	12.6	99.2
VG24-16	374	123865	1.4	14.8196	0.9	1.2813	2.2	0.1378	2.0	0.91	832.1	15.5	837.4	12.4	852.6	18.9	832.1	15.5	97.6
VG24-16	87	159675	1.2	15.1346	1.2	1.2707	2.1	0.1395	1.7	0.82	842.1	13.5	832.7	11.9	808.7	25.3	842.1	13.5	104.1
VG24-16	100	35293	1.2	14.6848	1.1	1.3290	2.2	0.1416	1.9	0.86	853.7	14.9	858.4	12.6	871.5	23.2	853.7	14.9	98.0
VG24-16	83	52824	1.3	14.6745	1.2	1.4107	1.9	0.1502	1.5	0.79	902.1	12.6	893.4	11.3	873.0	24.1	902.1	12.6	103.3
VG24-16	86	62378	2.5	13.9705	1.1	1.5310	2.5	0.1552	2.2	0.90	930.0	19.4	942.9	15.3	974.0	21.8	974.0	21.8	95.5
VG24-16	174	30652	8.0	13.8281	1.2	1.6766	2.2	0.1682	1.9	0.83	1002.3	17.4	999.7	14.3	994.9	25.2	994.9	25.2	100.7

ages for grains<1000 Ma based on 206Pb/238U values; ages for grains>1000 Ma based on 206Pb/207Pb

ACCEPTED MANUSCRIPT

Table 1 A. U-Pb geochronologic analyses from sample VG24-16 (cont) (n=187)

						Isotope ratios					Apparent ages (Ma)								
Analysis	U	206Pb	U/Th	206Pb*	±	207Pb*	±	206Pb*	±	error	206Pb*	±	207Pb*	±	206Pb*	±	Best age	±	Conc
	(ppm)	204Pb		207Pb*	(%)	235U*	(%)	238U	(%)	corr.	238U*	(Ma)	235U	(Ma)	207Pb*	(Ma)	(Ma)	(Ma)	(%)
VG24-16	169	25542	1.3	13.7647	0.8	1.5291	1.9	0.1527	1.7	0.91	916.2	14.6	942.1	11.6	1004.2	16.0	1004.2	16.0	91.2
VG24-16	169	71184	2.7	13.7451	0.9	1.5859	2.2	0.1582	2.0	0.91	946.6	17.8	964.7	13.9	1007.1	18.8	1007.1	18.8	94.0
VG24-16	309	15219	3.2	13.7189	1.1	1.6416	2.1	0.1634	1.8	0.86	975.7	16.3	986.3	13.3	1010.9	22.0	1010.9	22.0	96.5
VG24-16	611	101793	2.8	13.6676	1.0	1.5197	1.6	0.1507	1.3	0.80	904.9	11.1	938.3	10.1	1018.5	20.1	1018.5	20.1	88.8
VG24-16	472	166242	3.1	13.6143	0.9	1.5580	2.1	0.1539	1.9	0.90	922.8	16.2	953.7	13.0	1026.4	18.7	1026.4	18.7	89.9
VG24-16	497	90061	1.4	13.6007	1.2	1.6837	2.3	0.1662	2.0	0.86	990.9	18.5	1002.4	14.9	1028.5	24.1	1028.5	24.1	96.3
VG24-16	121	43252	0.7	13.5920	1.2	1.7455	2.4	0.1721	2.1	0.87	1023.9	19.8	1025.5	15.6	1029.7	24.3	1029.7	24.3	99.4
VG24-16	200	26949	1.2	13.5751	1.3	1.7229	2.2	0.1697	1.8	0.82	1010.5	16.9	1017.1	14.2	1032.3	25.8	1032.3	25.8	97.9
VG24-16	278	27321	3.8	13.5624	0.8	1.7281	1.8	0.1701	1.6	0.89	1012.4	14.8	1019.0	11.4	1034.2	16.1	1034.2	16.1	97.9
VG24-16	70	16790	5.0	13.5285	1.5	1.8485	2.2	0.1814	1.7	0.76	1074.9	16.9	1062.9	14.8	1039.2	29.3	1039.2	29.3	103.4
VG24-16	399	336333	3.9	13.4873	1.0	1.7744	2.1	0.1736	1.8	0.87	1032.2	17.1	1036.1	13.4	1045.4	20.8	1045.4	20.8	98.7
VG24-16	356	118806	1.4	13.3873	0.9	1.8212	2.5	0.1769	2.3	0.93	1050.1	22.1	1053.1	16.1	1060.4	18.6	1060.4	18.6	99.0
VG24-16	134	46390	1.9	13.3833	1.2	1.8313	2.3	0.1778	2.0	0.86	1055.1	19.1	1056.7	15.1	1061.0	23.8	1061.0	23.8	99.4
VG24-16	14	9922	1.7	13.3819	1.6	1.9228	2.7	0.1867	2.1	0.80	1103.5	21.6	1089.1	17.8	1061.2	32.4	1061.2	32.4	104.0
VG24-16	203	35863	2.3	13.3667	1.1	1.8583	2.2	0.1802	1.9	0.87	1068.2	18.8	1066.4	14.5	1063.5	22.0	1063.5	22.0	100.4
VG24-16	199	48012	2.9	13.3025	1.2	1.8995	1.9	0.1833	1.6	0.80	1085.2	15.6	1080.9	12.9	1073.2	23.3	1073.2	23.3	101.1
VG24-16	55	187710	2.2	13.2279	1.5	1.9981	2.0	0.1918	1.4	0.70	1131.0	14.8	1114.9	13.8	1084.5	29.4	1084.5	29.4	104.3
VG24-16	711	1198430	2.6	13.1977	1.1	1.8145	1.9	0.1738	1.5	0.81	1032.8	14.4	1050.7	12.1	1089.0	21.6	1089.0	21.6	94.8
VG24-16	441	1115453	2.7	13.1438	0.9	1.9655	2.4	0.1875	2.3	0.92	1107.6	23.0	1103.8	16.5	1097.2	18.9	1097.2	18.9	100.9
VG24-16	194	106275	1.3	13.0547	1.2	1.9534	1.9	0.1850	1.6	0.80	1094.4	15.8	1099.6	13.1	1110.8	23.1	1110.8	23.1	98.5
VG24-16	99	86270	2.3	13.0314	1.1	1.8974	1.9	0.1794	1.5	0.81	1063.8	15.2	1080.2	12.7	1114.4	22.2	1114.4	22.2	95.5
VG24-16	131	49859	2.6	12.9935	1.2	1.9541	2.4	0.1842	2.1	0.86	1090.1	20.7	1099.9	16.1	1120.2	24.0	1120.2	24.0	97.3

ages for grains<1000 Ma based on 206Pb/238U values; ages for grains>1000 Ma based on 206Pb/207Pb

ACCEPTED MANUSCRIPT

Table 1 A. U-Pb geochronologic analyses from sample VG24-16 (cont) (n=187)

						Isotope ratios					Apparent ages (Ma)								
Analysis	U	206Pb	U/Th	206Pb*	±	207Pb*	±	206Pb*	±	error	206Pb*	±	207Pb*	±	206Pb*	±	Best age	±	Conc
	(ppm)	204Pb		207Pb*	(%)	235U*	(%)	238U	(%)	corr.	238U*	(Ma)	235U	(Ma)	207Pb*	(Ma)	(Ma)	(Ma)	(%)
VG24-16	80	45253	4.0	12.9890	1.4	1.8335	2.3	0.1728	1.8	0.79	1027.5	17.1	1057.5	15.0	1120.9	27.9	1120.9	27.9	91.7
VG24-16	140	55991	1.2	12.9465	1.1	1.8448	2.3	0.1733	2.0	0.88	1030.3	18.8	1061.6	14.9	1127.4	21.8	1127.4	21.8	91.4
VG24-16	29	29555	2.7	12.9112	1.7	1.9574	2.5	0.1834	1.8	0.72	1085.4	17.6	1101.0	16.5	1132.9	34.1	1132.9	34.1	95.8
VG24-16	209	104768	2.2	12.8970	1.0	2.0482	1.8	0.1917	1.5	0.83	1130.4	15.7	1131.7	12.4	1135.0	20.2	1135.0	20.2	99.6
VG24-16	297	84359	1.5	12.8858	1.1	1.9984	2.6	0.1868	2.3	0.90	1104.2	23.4	1115.0	17.4	1136.8	22.3	1136.8	22.3	97.1
VG24-16	248	213255	3.4	12.8842	1.3	1.9435	2.1	0.1817	1.7	0.78	1076.2	16.4	1096.2	14.3	1137.0	26.7	1137.0	26.7	94.6
VG24-16	47	19046	1.5	12.8807	1.6	2.0964	2.4	0.1959	1.8	0.74	1153.4	18.7	1147.6	16.6	1137.6	32.4	1137.6	32.4	101.4
VG24-16	204	467648	1.7	12.8162	1.2	1.9846	2.1	0.1846	1.7	0.81	1091.8	16.8	1110.3	14.0	1147.5	24.2	1147.5	24.2	95.1
VG24-16	593	91663	1.9	12.7180	1.1	2.0877	2.0	0.1927	1.7	0.83	1135.7	17.3	1144.8	13.7	1162.8	22.0	1162.8	22.0	97.7
VG24-16	274	89194	3.7	12.6956	1.0	2.1494	2.0	0.1980	1.7	0.86	1164.5	18.1	1164.8	13.7	1166.3	19.8	1166.3	19.8	99.9
VG24-16	144	71498	1.9	12.5698	1.2	2.0294	2.4	0.1851	2.0	0.87	1094.7	20.6	1125.4	16.0	1186.0	23.0	1186.0	23.0	92.3
VG24-16	299	77780	2.9	12.4356	1.1	2.2658	2.5	0.2044	2.2	0.89	1199.2	24.2	1201.7	17.5	1207.2	21.9	1207.2	21.9	99.3
VG24-16	243	100042	2.1	12.3609	1.3	2.2972	2.5	0.2060	2.1	0.85	1207.7	23.3	1211.4	17.5	1219.0	25.2	1219.0	25.2	99.1
VG24-16	119	23733	0.8	12.0639	1.3	2.3381	2.2	0.2047	1.9	0.83	1200.3	20.4	1223.9	16.0	1266.7	24.6	1266.7	24.6	94.8
VG24-16	195	142043	2.1	12.0248	1.2	2.0102	2.2	0.1754	1.9	0.84	1041.7	18.2	1119.0	15.2	1273.0	23.5	1273.0	23.5	81.8
VG24-16	282	90334	3.1	11.9802	1.1	2.4769	1.9	0.2153	1.5	0.82	1257.0	17.6	1265.3	13.6	1280.2	20.8	1280.2	20.8	98.2
VG24-16	65	36540	1.0	11.8272	1.4	2.6883	2.5	0.2307	2.1	0.84	1338.2	25.9	1325.2	18.9	1305.2	26.8	1305.2	26.8	102.5
VG24-16	8	4947	2.2	11.6485	2.8	2.4237	3.7	0.2049	2.4	0.66	1201.3	26.8	1249.7	26.5	1334.7	53.4	1334.7	53.4	90.0
VG24-16	131	167264	1.5	11.5884	1.2	2.7535	2.1	0.2315	1.7	0.81	1342.5	21.0	1343.0	15.9	1344.7	24.1	1344.7	24.1	99.8
VG24-16	761	134319	0.8	11.2294	1.0	2.9045	1.8	0.2367	1.6	0.85	1369.3	19.2	1383.1	13.8	1405.3	18.3	1405.3	18.3	97.4
VG24-16	275	135283	1.1	11.0846	1.2	2.8750	2.2	0.2312	1.9	0.85	1340.9	22.6	1375.4	16.5	1430.1	22.0	1430.1	22.0	93.8
VG24-16	368	115447	2.5	11.0468	1.0	2.9105	2.4	0.2333	2.2	0.92	1351.7	26.6	1384.6	18.0	1436.6	18.2	1436.6	18.2	94.1

ages for grains<1000 Ma based on 206Pb/238U values; ages for grains>1000 Ma based on 206Pb/207Pb

ACCEPTED MANUSCRIPT

Table 1 A. U-Pb geochronologic analyses from sample VG24-16 (cont) (n=187)

						Isotope ratios					Apparent ages (Ma)								
Analysis	U	206Pb	U/Th	206Pb*	±	207Pb*	±	206Pb*	±	error	206Pb*	±	207Pb*	±	206Pb*	±	Best age	±	Conc
	(ppm)	204Pb		207Pb*	(%)	235U*	(%)	238U	(%)	corr.	238U*	(Ma)	235U	(Ma)	207Pb*	(Ma)	(Ma)	(Ma)	(%)
VG24-16	261	67691	1.2	11.0237	1.0	3.0769	2.1	0.2461	1.8	0.87	1418.4	23.1	1426.9	16.1	1440.6	19.9	1440.6	19.9	98.5
VG24-16	206	966247	1.8	11.0159	0.9	3.0022	2.0	0.2400	1.7	0.88	1386.5	21.4	1408.2	14.9	1441.9	18.0	1441.9	18.0	96.2
VG24-16	261	102953	2.3	10.8964	1.2	3.3281	2.5	0.2631	2.2	0.88	1505.8	30.1	1487.7	19.8	1462.7	22.6	1462.7	22.6	102.9
VG24-16	299	33645	1.7	9.1015	1.0	4.9243	2.1	0.3252	1.9	0.88	1815.1	29.5	1806.4	17.8	1797.3	18.1	1797.3	18.1	101.0
VG24-16	178	601593	1.1	8.9168	1.1	5.0182	2.2	0.3247	1.8	0.85	1812.5	29.2	1822.4	18.4	1834.5	20.7	1834.5	20.7	98.8
VG24-16	309	113664	0.8	8.8263	0.8	4.5597	1.9	0.2920	1.7	0.91	1651.6	24.7	1741.9	15.5	1853.0	13.8	1853.0	13.8	89.1
VG24-16	356	262464	1.5	8.6976	0.8	5.1544	2.3	0.3253	2.2	0.94	1815.5	34.3	1845.1	19.5	1879.5	13.8	1879.5	13.8	96.6
VG24-16	294	97382	1.1	8.4652	0.8	5.6202	1.8	0.3452	1.6	0.90	1911.7	26.7	1919.2	15.4	1928.1	13.7	1928.1	13.7	99.1
VG24-16	169	315899	1.0	5.7058	1.0	11.6241	1.7	0.4812	1.3	0.82	2532.7	28.2	2574.6	15.4	2608.5	15.9	2608.5	15.9	97.1

ages for grains<1000 Ma based on 206Pb/238U values; ages for grains>1000 Ma based on 206Pb/207Pb

Table 1 B. U-Pb geochronologic analyses from sample VLP001-17 (n=106)

						Isotope ratios					Apparent ages (Ma)								
Analysis	U	206Pb	U/Th	206Pb*	±	207Pb*	±	206Pb*	±	error	206Pb*	±	207Pb*	±	206Pb*	±	Best age	±	Conc
	(ppm)	204Pb		207Pb*	(%)	235U*	(%)	238U	(%)	corr.	238U*	(Ma)	235U	(Ma)	207Pb*	(Ma)	(Ma)	(Ma)	(%)
VLP001-17	120	17936	1.9	18.2704	3.7	0.1209	4.2	0.0160	2.0	0.47	102.5	2.0	115.9	4.6	400.4	83.9	102.5	2.0	NA
VLP001-17	414	55038	1.0	19.8871	1.4	0.1151	1.8	0.0166	1.1	0.61	106.2	1.2	110.6	1.9	207.1	33.2	106.2	1.2	NA
VLP001-17	914	11906	1.2	17.0468	1.5	0.1358	1.9	0.0168	1.2	0.63	107.4	1.3	129.3	2.3	553.6	32.6	107.4	1.3	NA
VLP001-17	234	3209	1.6	22.5421	5.7	0.1028	6.0	0.0168	1.8	0.30	107.5	1.9	99.4	5.7	NA	NA	107.5	1.9	NA
VLP001-17	503	45196	1.5	20.2397	1.7	0.1159	2.4	0.0170	1.7	0.72	108.8	1.8	111.3	2.5	166.2	38.6	108.8	1.8	NA
VLP001-17	223	77476	1.4	18.7374	2.6	0.1262	3.1	0.0172	1.6	0.53	109.6	1.8	120.6	3.5	343.5	59.4	109.6	1.8	NA

ages for grains<1000 Ma based on 206Pb/238U values; ages for grains>1000 Ma based on 206Pb/207Pb

ACCEPTED MANUSCRIPT

Table 1 B. U-Pb geochronologic analyses from sample VLP001-17 (cont) (n=106)

				Isotope ratios							Apparent ages (Ma)								
Analysis	U	206Pb	U/Th	206Pb*	±	207Pb*	±	206Pb*	±	error	206Pb*	±	207Pb*	±	206Pb*	±	Best age	±	Conc
	(ppm)	204Pb		207Pb*	(%)	235U*	(%)	238U	(%)	corr.	238U*	(Ma)	235U	(Ma)	207Pb*	(Ma)	(Ma)	(Ma)	(%)
VLP001-17	193	10544	1.4	18.9213	1.4	0.1250	1.9	0.0172	1.3	0.68	109.7	1.4	119.6	2.1	321.4	31.1	109.7	1.4	NA
VLP001-17	433	15399	1.5	19.0962	1.9	0.1240	2.4	0.0172	1.5	0.63	109.8	1.7	118.7	2.7	300.5	43.5	109.8	1.7	NA
VLP001-17	382	7336	1.8	21.1992	2.1	0.1119	2.8	0.0172	1.9	0.68	110.0	2.1	107.7	2.9	56.9	49.0	110.0	2.1	NA
VLP001-17	562	11546	0.9	21.1320	1.3	0.1131	1.8	0.0173	1.1	0.65	110.8	1.2	108.8	1.8	64.4	31.9	110.8	1.2	NA
VLP001-17	170	11078	1.7	19.2345	2.7	0.1257	3.0	0.0175	1.5	0.49	112.1	1.7	120.2	3.5	284.0	60.6	112.1	1.7	NA
VLP001-17	178	7987	0.9	12.1384	2.6	0.2016	3.7	0.0178	2.7	0.72	113.4	3.0	186.5	6.3	1253.8	50.7	113.4	3.0	NA
VLP001-17	195	11928	1.9	18.0292	2.2	0.1358	2.9	0.0178	1.9	0.65	113.5	2.1	129.3	3.5	430.0	49.4	113.5	2.1	NA
VLP001-17	434	4412	1.0	16.1289	2.3	0.1520	2.8	0.0178	1.5	0.55	113.7	1.7	143.7	3.7	673.2	49.7	113.7	1.7	NA
VLP001-17	73	2854	1.4	11.7642	4.2	0.2089	4.7	0.0178	2.3	0.48	113.9	2.6	192.6	8.3	1314.8	80.5	113.9	2.6	NA
VLP001-17	87	2023	1.4	25.4933	4.0	0.1011	5.7	0.0187	4.0	0.71	119.5	4.7	97.8	5.3	NA	NA	119.5	4.7	NA
VLP001-17	293	55100	1.9	21.3427	1.9	0.1230	2.6	0.0191	1.7	0.66	121.7	2.1	117.8	2.9	40.8	46.5	121.7	2.1	NA
VLP001-17	375	2128	2.0	17.1806	2.0	0.1533	2.5	0.0191	1.5	0.60	122.0	1.8	144.8	3.3	536.5	42.9	122.0	1.8	NA
VLP001-17	174	4751	2.1	18.1204	3.7	0.1521	5.2	0.0200	3.6	0.70	127.6	4.6	143.7	6.9	418.8	82.6	127.6	4.6	NA
VLP001-17	182	6644	2.2	17.4308	3.2	0.1726	4.5	0.0218	3.2	0.70	139.2	4.4	161.7	6.7	504.8	70.5	139.2	4.4	NA
VLP001-17	194	1598	1.0	20.7949	9.4	0.1500	9.9	0.0226	3.1	0.32	144.2	4.5	141.9	13.1	102.6	222.6	144.2	4.5	NA
VLP001-17	1065	228325	0.8	20.0970	0.6	0.1590	1.3	0.0232	1.1	0.90	147.8	1.7	149.9	1.8	182.7	13.1	147.8	1.7	NA
VLP001-17	414	32858	1.0	16.7084	2.2	0.1974	2.9	0.0239	1.8	0.63	152.5	2.7	182.9	4.8	597.2	48.6	152.5	2.7	NA
VLP001-17	447	15286	0.8	20.3595	1.4	0.1635	1.9	0.0242	1.3	0.67	153.8	2.0	153.8	2.7	152.4	33.4	153.8	2.0	NA
VLP001-17	206	7794	0.8	15.8653	2.0	0.3424	2.6	0.0394	1.7	0.64	249.2	4.0	299.0	6.7	708.3	42.3	249.2	4.0	NA
VLP001-17	378	117508	2.6	18.9876	1.2	0.2866	1.7	0.0395	1.2	0.71	249.6	3.0	255.8	3.9	313.5	28.0	249.6	3.0	NA
VLP001-17	281	4849	1.8	16.3291	1.5	0.3448	1.7	0.0409	1.0	0.55	258.1	2.4	300.8	4.5	646.8	31.4	258.1	2.4	NA
VLP001-17	91	19896	2.3	19.7654	2.1	0.2860	2.6	0.0410	1.5	0.59	259.1	3.9	255.4	5.9	221.3	48.6	259.1	3.9	NA

ages for grains<1000 Ma based on 206Pb/238U values; ages for grains>1000 Ma based on 206Pb/207Pb

ACCEPTED MANUSCRIPT

Table 1 B. U-Pb geochronologic analyses from sample VLP001-17 (cont) (n=106)

						Isotope ratios					Apparent ages (Ma)								
Analysis	U	206Pb	U/Th	206Pb*	±	207Pb*	±	206Pb*	±	error	206Pb*	±	207Pb*	±	206Pb*	±	Best age	±	Conc
	(ppm)	204Pb		207Pb*	(%)	235U*	(%)	238U	(%)	corr.	238U*	(Ma)	235U	(Ma)	207Pb*	(Ma)	(Ma)	(Ma)	(%)
VLP001-17	210	19187	1.3	18.1638	1.5	0.3113	2.0	0.0410	1.3	0.65	259.2	3.3	275.2	4.8	413.4	33.8	259.2	3.3	NA
VLP001-17	272	31271	1.0	19.2058	1.1	0.3000	1.4	0.0418	0.8	0.62	264.0	2.2	266.4	3.2	287.4	24.4	264.0	2.2	NA
VLP001-17	129	2588	2.0	11.6196	8.4	0.4986	8.6	0.0420	1.9	0.22	265.4	4.9	410.7	29.1	1338.7	162.5	265.4	4.9	NA
VLP001-17	194	7186	2.4	20.0485	1.2	0.2890	1.7	0.0420	1.2	0.69	265.5	3.1	257.8	3.9	188.3	28.8	265.5	3.1	NA
VLP001-17	156	4973	1.1	18.4700	1.9	0.3148	2.3	0.0422	1.3	0.56	266.4	3.4	277.9	5.6	376.0	42.9	266.4	3.4	NA
VLP001-17	205	6569	1.9	19.2891	1.4	0.3017	2.3	0.0422	1.8	0.79	266.6	4.7	267.7	5.4	277.5	32.3	266.6	4.7	NA
VLP001-17	429	25563	2.8	19.1821	1.3	0.3040	2.2	0.0423	1.9	0.83	267.1	4.9	269.5	5.3	290.2	28.7	267.1	4.9	NA
VLP001-17	102	5174	2.3	16.8738	2.3	0.3469	2.7	0.0425	1.4	0.54	268.1	3.8	302.4	7.1	575.8	49.5	268.1	3.8	NA
VLP001-17	98	71429	0.8	16.9648	2.7	0.3454	3.2	0.0425	1.6	0.51	268.4	4.3	301.3	8.2	564.1	59.0	268.4	4.3	NA
VLP001-17	35	52911	1.9	19.0011	4.1	0.3088	6.7	0.0426	5.3	0.79	268.8	13.9	273.2	16.1	311.8	94.0	268.8	13.9	NA
VLP001-17	245	52530	2.2	19.4945	1.4	0.3024	2.5	0.0428	2.0	0.82	270.0	5.3	268.2	5.8	253.2	32.1	270.0	5.3	NA
VLP001-17	1048	75716	1.3	18.6614	0.7	0.3161	1.3	0.0428	1.1	0.86	270.2	3.0	278.9	3.2	352.7	14.9	270.2	3.0	NA
VLP001-17	282	8555	1.3	19.1246	1.5	0.3099	2.1	0.0430	1.4	0.69	271.4	3.8	274.1	4.9	297.1	34.0	271.4	3.8	NA
VLP001-17	157	7888	1.6	19.2925	1.5	0.3078	1.9	0.0431	1.2	0.64	271.9	3.2	272.5	4.5	277.1	33.3	271.9	3.2	NA
VLP001-17	23	747	1.8	31.3595	17.7	0.1901	18.1	0.0433	3.7	0.20	273.0	9.9	176.7	29.3	NA	NA	273.0	9.9	NA
VLP001-17	410	8626	1.5	18.0594	1.3	0.3307	1.8	0.0433	1.2	0.68	273.5	3.3	290.1	4.6	426.3	29.8	273.5	3.3	NA
VLP001-17	154	10368	1.7	19.8892	1.8	0.3048	2.5	0.0440	1.7	0.69	277.5	4.6	270.2	5.8	206.9	41.4	277.5	4.6	NA
VLP001-17	35	1558	1.0	18.1271	3.4	0.3366	3.8	0.0443	1.6	0.44	279.2	4.5	294.6	9.6	418.0	75.8	279.2	4.5	NA
VLP001-17	368	7022	1.0	20.3815	1.5	0.2997	1.9	0.0443	1.1	0.62	279.5	3.1	266.1	4.3	149.9	34.0	279.5	3.1	NA
VLP001-17	205	7975	2.6	17.2122	1.5	0.3602	2.2	0.0450	1.5	0.71	283.6	4.3	312.4	5.8	532.5	33.1	283.6	4.3	NA
VLP001-17	456	16650	1.6	18.9930	0.9	0.3276	1.8	0.0451	1.6	0.86	284.7	4.4	287.7	4.6	312.8	21.2	284.7	4.4	NA
VLP001-17	621	72131	2.1	19.0728	1.0	0.3289	1.5	0.0455	1.2	0.77	287.0	3.3	288.8	3.9	303.2	22.4	287.0	3.3	NA

ages for grains<1000 Ma based on 206Pb/238U values; ages for grains>1000 Ma based on 206Pb/207Pb

ACCEPTED MANUSCRIPT

Table 1 B. U-Pb geochronologic analyses from sample VLP001-17 (cont) (n=106)

						Isotope ratios					Apparent ages (Ma)								
Analysis	U	206Pb	U/Th	206Pb*	±	207Pb*	±	206Pb*	±	error	206Pb*	±	207Pb*	±	206Pb*	±	Best age	±	Conc
	(ppm)	204Pb		207Pb*	(%)	235U*	(%)	238U	(%)	corr.	238U*	(Ma)	235U	(Ma)	207Pb*	(Ma)	(Ma)	(Ma)	(%)
VLP001-17	213	6807	3.3	17.7634	2.4	0.3565	3.0	0.0460	1.8	0.59	289.6	5.0	309.6	8.0	463.1	53.4	289.6	5.0	NA
VLP001-17	588	12323	2.1	19.9613	0.9	0.3234	1.3	0.0468	1.0	0.77	295.1	2.9	284.5	3.3	198.5	19.9	295.1	2.9	NA
VLP001-17	691	11389	2.0	17.8888	0.9	0.3643	1.6	0.0473	1.3	0.81	297.8	3.7	315.4	4.3	447.4	20.7	297.8	3.7	NA
VLP001-17	521	62436	2.9	19.2037	0.9	0.3430	1.5	0.0478	1.2	0.80	300.9	3.4	299.4	3.8	287.6	20.0	300.9	3.4	NA
VLP001-17	508	154418	3.3	18.8684	0.8	0.3625	1.4	0.0496	1.1	0.80	312.3	3.4	314.1	3.7	327.7	18.7	312.3	3.4	NA
VLP001-17	338	8565	2.4	19.4395	1.5	0.3623	2.2	0.0511	1.6	0.74	321.3	5.0	313.9	5.8	259.7	33.6	321.3	5.0	NA
VLP001-17	60	2902	3.7	20.5127	5.1	0.3627	6.4	0.0540	3.8	0.60	339.0	12.6	314.3	17.3	134.8	120.3	339.0	12.6	NA
VLP001-17	349	25739	0.7	17.8239	1.0	0.4561	1.6	0.0590	1.3	0.77	369.5	4.5	381.6	5.1	455.5	22.7	369.5	4.5	NA
VLP001-17	252	8011	1.9	18.9691	2.0	0.4468	2.4	0.0615	1.3	0.54	384.7	4.8	375.0	7.5	315.6	45.9	384.7	4.8	NA
VLP001-17	842	92914	1.6	18.2547	0.9	0.4727	1.7	0.0626	1.4	0.83	391.4	5.2	393.0	5.4	402.3	21.0	391.4	5.2	NA
VLP001-17	314	75017	1.6	17.6549	1.3	0.4894	1.8	0.0627	1.3	0.71	392.0	4.9	404.5	6.1	476.6	28.5	392.0	4.9	NA
VLP001-17	608	153448	2.6	17.3073	0.8	0.5175	1.7	0.0650	1.4	0.86	405.9	5.6	423.5	5.7	520.4	18.5	405.9	5.6	78.0
VLP001-17	610	33871	2.1	17.7079	0.9	0.5063	1.7	0.0651	1.4	0.83	406.3	5.5	416.0	5.7	470.0	20.5	406.3	5.5	86.4
VLP001-17	243	15925	1.1	18.0184	1.2	0.5040	1.5	0.0659	0.9	0.60	411.4	3.6	414.4	5.1	431.4	27.0	411.4	3.6	95.4
VLP001-17	353	40172	19.3	18.0548	1.2	0.5621	2.0	0.0736	1.6	0.78	458.1	6.9	452.9	7.2	426.9	27.6	458.1	6.9	107.3
VLP001-17	815	1664946	1.7	17.5115	1.0	0.5873	2.1	0.0746	1.8	0.88	463.9	8.2	469.1	7.8	494.7	21.9	463.9	8.2	93.8
VLP001-17	565	305738	1.7	17.9295	0.8	0.5909	1.5	0.0769	1.2	0.84	477.4	5.6	471.4	5.5	442.4	17.9	477.4	5.6	107.9
VLP001-17	642	58510	1.2	17.3896	0.9	0.6117	1.7	0.0772	1.4	0.85	479.3	6.6	484.6	6.4	510.0	19.2	479.3	6.6	94.0
VLP001-17	66	4047	1.9	17.8969	3.6	0.6349	3.9	0.0825	1.6	0.40	510.7	7.8	499.2	15.6	446.4	80.4	510.7	7.8	114.4
VLP001-17	179	33868	2.7	17.9195	1.4	0.6506	2.0	0.0846	1.5	0.73	523.5	7.5	508.8	8.2	443.6	31.2	523.5	7.5	118.0
VLP001-17	228	7993	2.8	17.4053	1.3	0.6864	2.1	0.0867	1.6	0.78	535.9	8.3	530.7	8.6	508.0	29.0	535.9	8.3	105.5
VLP001-17	235	17737	3.7	17.4931	1.2	0.6877	2.1	0.0873	1.8	0.83	539.5	9.1	531.4	8.8	497.0	26.0	539.5	9.1	108.6

ages for grains<1000 Ma based on 206Pb/238U values; ages for grains>1000 Ma based on 206Pb/207Pb

ACCEPTED MANUSCRIPT

Table 1 B. U-Pb geochronologic analyses from sample VLP001-17 (cont) (n=106)

						Isotope ratios					Apparent ages (Ma)								
Analysis	U	206Pb	U/Th	206Pb*	±	207Pb*	±	206Pb*	±	error	206Pb*	±	207Pb*	±	206Pb*	±	Best age	±	Conc
	(ppm)	204Pb		207Pb*	(%)	235U*	(%)	238U	(%)	corr.	238U*	(Ma)	235U	(Ma)	207Pb*	(Ma)	(Ma)	(Ma)	(%)
VLP001-17	318	20905	6.3	17.2458	1.0	0.7087	1.7	0.0887	1.4	0.82	547.7	7.3	544.0	7.1	528.3	21.5	547.7	7.3	103.7
VLP001-17	328	91414	2.9	15.7872	1.2	0.7748	1.7	0.0888	1.2	0.71	548.1	6.3	582.5	7.4	718.8	25.0	548.1	6.3	76.3
VLP001-17	305	706485	1.7	16.1053	1.2	0.7651	1.6	0.0894	1.1	0.70	552.0	6.1	577.0	7.2	676.3	25.0	552.0	6.1	81.6
VLP001-17	238	14488	0.8	17.3715	1.3	0.7228	1.9	0.0911	1.4	0.72	562.0	7.4	552.3	8.2	512.3	29.3	562.0	7.4	109.7
VLP001-17	620	61174	6.0	17.1163	1.0	0.7336	1.9	0.0911	1.6	0.84	562.1	8.5	558.7	8.1	544.7	22.5	562.1	8.5	103.2
VLP001-17	378	188725	1.2	16.5982	0.7	0.7803	1.4	0.0940	1.1	0.84	579.0	6.3	585.6	6.0	611.5	15.7	579.0	6.3	94.7
VLP001-17	160	41165	5.1	14.3789	1.3	0.9032	1.8	0.0942	1.3	0.71	580.5	7.2	653.4	8.8	914.1	26.4	580.5	7.2	63.5
VLP001-17	326	35620	1.6	16.9231	1.0	0.7800	1.7	0.0958	1.3	0.80	589.6	7.5	585.5	7.4	569.5	21.7	589.6	7.5	103.5
VLP001-17	267	28242	1.0	16.5574	0.8	0.8163	1.4	0.0981	1.1	0.80	603.1	6.2	606.0	6.2	616.8	17.5	603.1	6.2	97.8
VLP001-17	402	92865	3.2	16.7246	0.8	0.8083	1.6	0.0981	1.3	0.84	603.2	7.6	601.5	7.1	595.1	18.1	603.2	7.6	101.4
VLP001-17	832	369886	21.1	16.5473	0.6	0.8424	1.2	0.1011	1.1	0.89	621.1	6.4	620.5	5.6	618.1	12.2	621.1	6.4	100.5
VLP001-17	597	1441196	13.5	16.0254	0.8	0.8866	1.6	0.1031	1.4	0.86	632.5	8.3	644.5	7.6	686.9	17.2	632.5	8.3	92.1
VLP001-17	128	12601	1.6	15.2767	1.3	0.9470	1.7	0.1050	1.1	0.66	643.5	6.7	676.6	8.2	788.2	26.4	643.5	6.7	81.6
VLP001-17	193	31783	1.5	16.3573	1.1	0.8933	1.7	0.1060	1.3	0.77	649.6	8.2	648.1	8.3	643.1	23.9	649.6	8.2	101.0
VLP001-17	157	37743	3.6	15.8244	1.0	0.9333	1.6	0.1072	1.3	0.80	656.3	8.1	669.4	7.9	713.8	20.5	656.3	8.1	91.9
VLP001-17	182	16442	2.5	15.2048	1.3	1.0016	2.2	0.1105	1.8	0.81	675.6	11.4	704.6	11.2	798.1	27.1	675.6	11.4	84.7
VLP001-17	89	11259	1.1	15.3696	1.3	1.0028	2.0	0.1118	1.4	0.73	683.4	9.3	705.2	9.9	775.4	27.9	683.4	9.3	88.1
VLP001-17	334	30881	5.9	14.2650	0.8	1.2464	1.4	0.1290	1.1	0.81	782.2	8.3	821.8	7.8	930.5	16.6	782.2	8.3	84.1
VLP001-17	409	21332248	3.4	13.3609	0.5	1.8699	1.2	0.1813	1.1	0.93	1073.9	11.3	1070.5	8.1	1063.5	9.4	1063.5	9.4	101.0
VLP001-17	132	181052	2.8	13.3186	0.9	1.8244	1.7	0.1763	1.5	0.85	1046.8	14.4	1054.3	11.5	1069.9	18.4	1069.9	18.4	97.8
VLP001-17	106	63213	2.0	13.1467	1.2	1.9405	2.0	0.1851	1.6	0.81	1094.8	16.4	1095.2	13.4	1095.9	23.4	1095.9	23.4	99.9
VLP001-17	97	24048	2.2	13.0823	1.2	1.9312	1.9	0.1833	1.4	0.76	1085.0	14.1	1091.9	12.4	1105.7	24.0	1105.7	24.0	98.1

ages for grains<1000 Ma based on 206Pb/238U values; ages for grains>1000 Ma based on 206Pb/207Pb

ACCEPTED MANUSCRIPT

Table 1 B. U-Pb geochronologic analyses from sample VLP001-17 (cont) (n=106)

						Isotope ratios					Apparent ages (Ma)								
Analysis	U	206Pb	U/Th	206Pb*	±	207Pb*	±	206Pb*	±	error	206Pb*	±	207Pb*	±	206Pb*	±	Best age	±	Conc
	(ppm)	204Pb		207Pb*	(%)	235U*	(%)	238U	(%)	corr.	238U*	(Ma)	235U	(Ma)	207Pb*	(Ma)	(Ma)	(Ma)	(%)
VLP001-17	60	26314	1.8	12.8546	1.3	2.0026	1.7	0.1868	1.2	0.68	1103.9	12.0	1116.4	11.8	1140.7	25.2	1140.7	25.2	96.8
VLP001-17	266	101665	1.4	12.5548	0.7	2.2235	1.1	0.2025	0.9	0.81	1189.0	10.0	1188.5	8.0	1187.5	13.3	1187.5	13.3	100.1
VLP001-17	83	39104	1.5	12.5183	1.2	2.0107	1.8	0.1826	1.3	0.73	1081.3	13.3	1119.1	12.4	1193.2	24.6	1193.2	24.6	90.6
VLP001-17	49	3341	2.2	12.3348	1.0	1.9195	2.2	0.1718	1.9	0.88	1022.0	18.1	1087.9	14.6	1222.3	20.6	1222.3	20.6	83.6
VLP001-17	241	63172	2.6	11.4044	0.7	2.8114	1.6	0.2326	1.4	0.89	1348.3	17.5	1358.6	12.1	1374.7	14.3	1374.7	14.3	98.1
VLP001-17	261	69840	1.3	11.0092	0.7	3.0139	1.6	0.2408	1.4	0.89	1390.6	17.8	1411.2	12.3	1442.3	14.3	1442.3	14.3	96.4
VLP001-17	120	304235	1.1	9.3129	0.9	4.4229	1.7	0.2989	1.5	0.85	1685.7	21.7	1716.6	14.2	1754.6	16.4	1754.6	16.4	96.1
VLP001-17	139	42610	1.2	9.1907	0.9	4.4828	1.6	0.2989	1.3	0.83	1686.1	19.5	1727.8	13.2	1778.7	16.4	1778.7	16.4	94.8
VLP001-17	193	95354	1.0	7.8383	0.7	6.4214	1.3	0.3652	1.1	0.83	2006.8	18.9	2035.2	11.6	2064.1	13.0	2064.1	13.0	97.2
VLP001-17	325	300668	13.5	5.2138	0.5	13.3860	1.0	0.5064	0.9	0.89	2641.2	18.8	2707.3	9.3	2756.9	7.5	2756.9	7.5	95.8
VLP001-17	234	30733	0.9	5.2035	0.7	11.7247	1.9	0.4427	1.8	0.92	2362.6	34.8	2582.7	17.8	2760.2	12.0	2760.2	12.0	85.6
VLP001-17	407	520201	2.1	5.1376	0.6	13.5228	1.5	0.5041	1.4	0.92	2631.4	30.5	2716.9	14.6	2781.1	10.0	2781.1	10.0	94.6

ages for grains<1000 Ma based on 206Pb/238U values; ages for grains>1000 Ma based on 206Pb/207Pb

ACCEPTED MANUSCRIPT

Figure 1

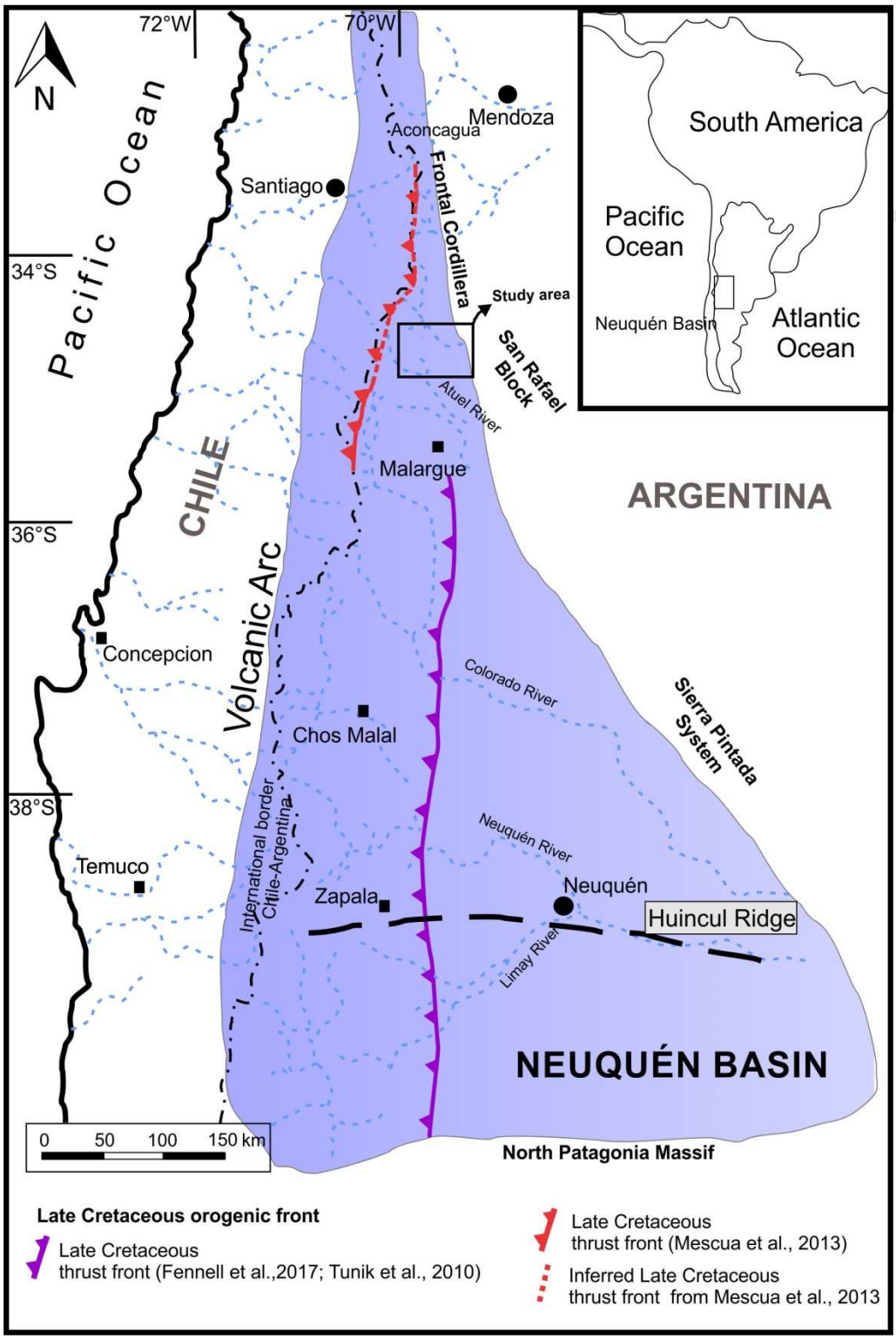
72°W
70°W
N
Pacific Ocean
34°S
36°S
38°S
CHILE
ARGENTINA
Mendoza
Aconcagua
Santiago
Frontal Cordillera
Study area
San Rafael Block
Atuel River
Malargue
Volcanic Arc
Concepcion
Colorado River
Sierra Pintada System
Chos Malal
International border Chile-Argentina
Neuquén River
Temuco
Zapala
Neuquén
Huincul Ridge
Limay River
NEUQUÉN BASIN
North Patagonia Massif
0 50 100 150 km
South America
Pacific Ocean
Neuquén Basin
Atlantic Ocean
Late Cretaceous orogenic front
Late Cretaceous thrust front (Fennell et al.,2017; Tunik et al., 2010)
Late Cretaceous thrust front (Mescua et al., 2013)
Inferred Late Cretaceous thrust front from Mescua et al., 2013

Figure 2

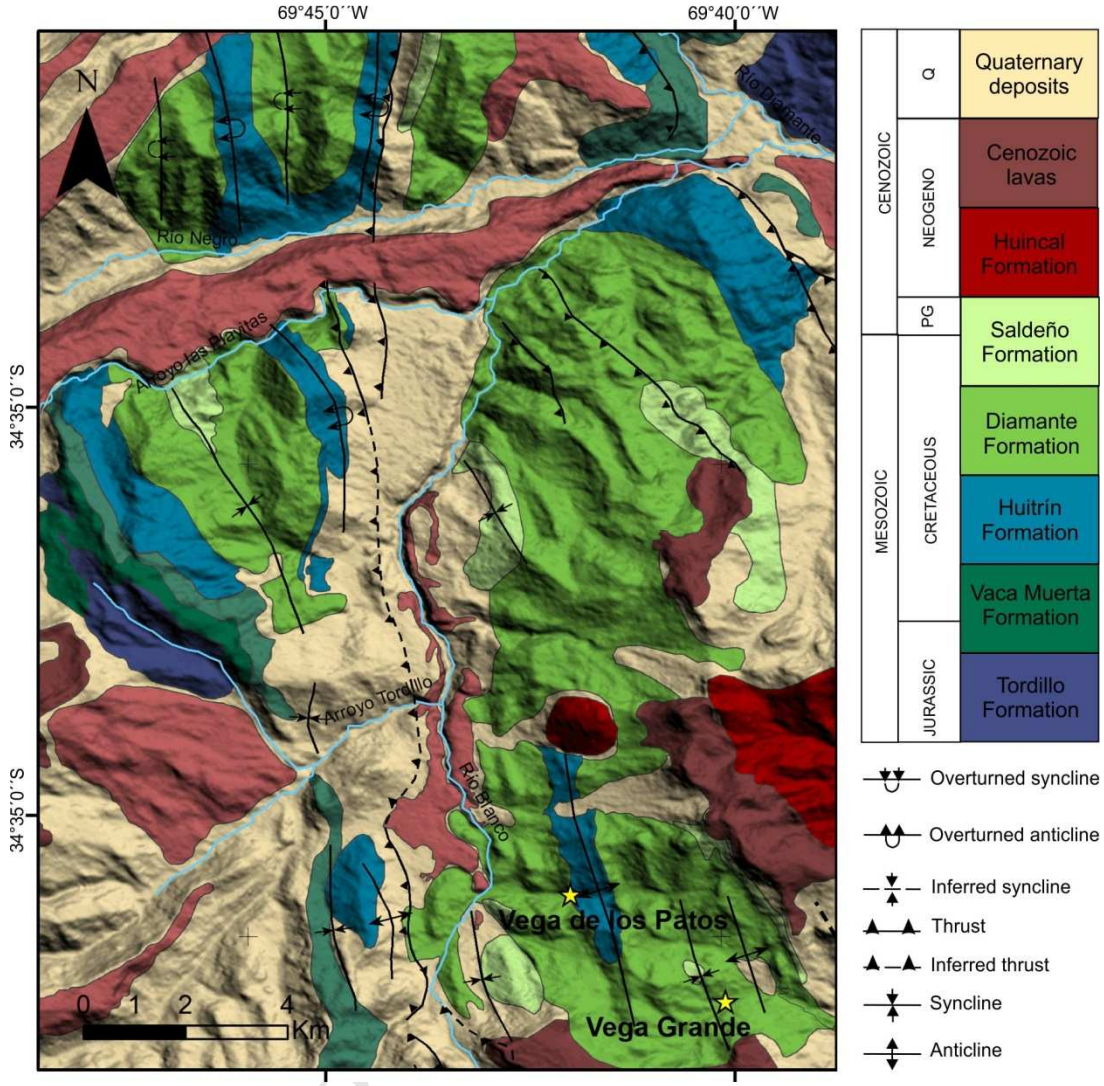

ACCEPTED

Figure 3

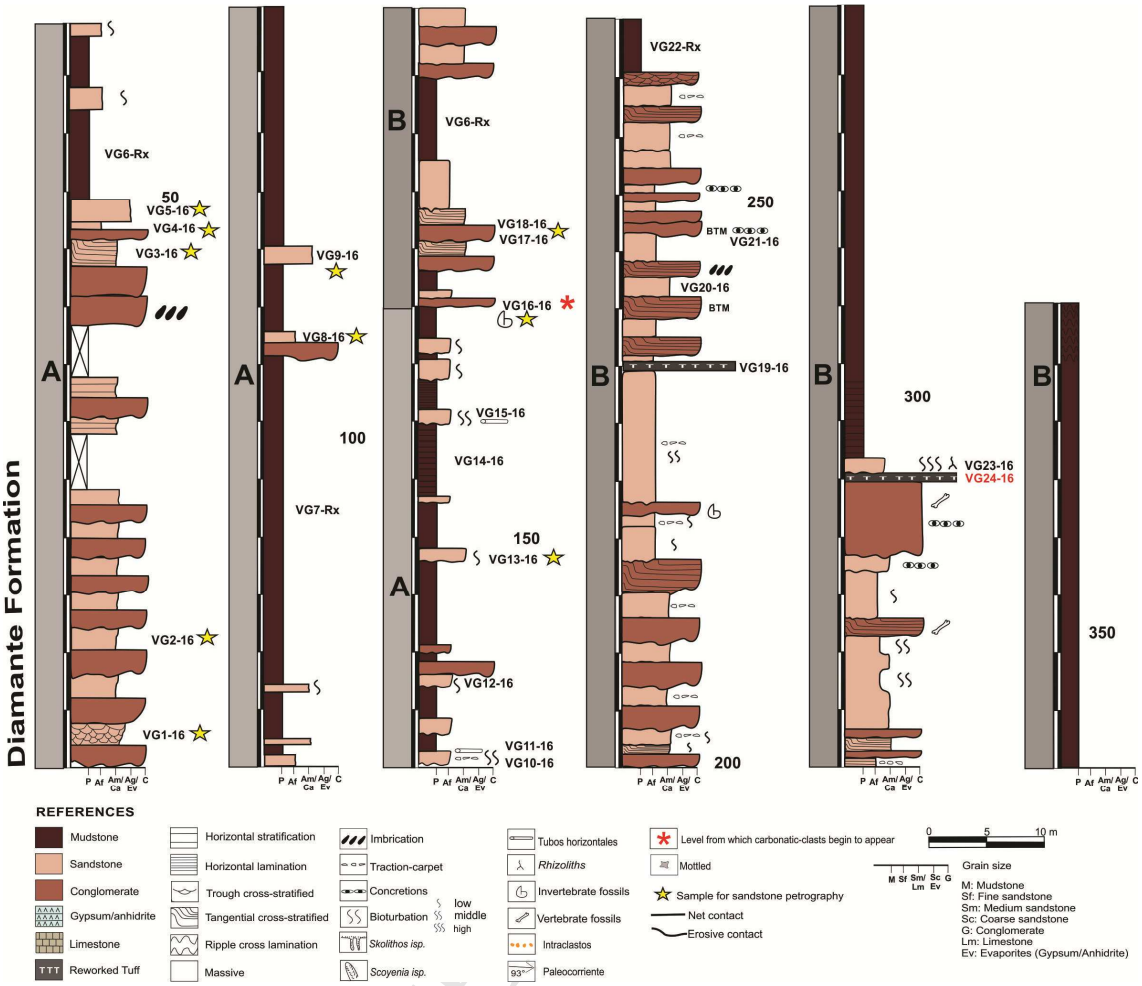

ACCEPTED MANUSCRIPT

Figure 4

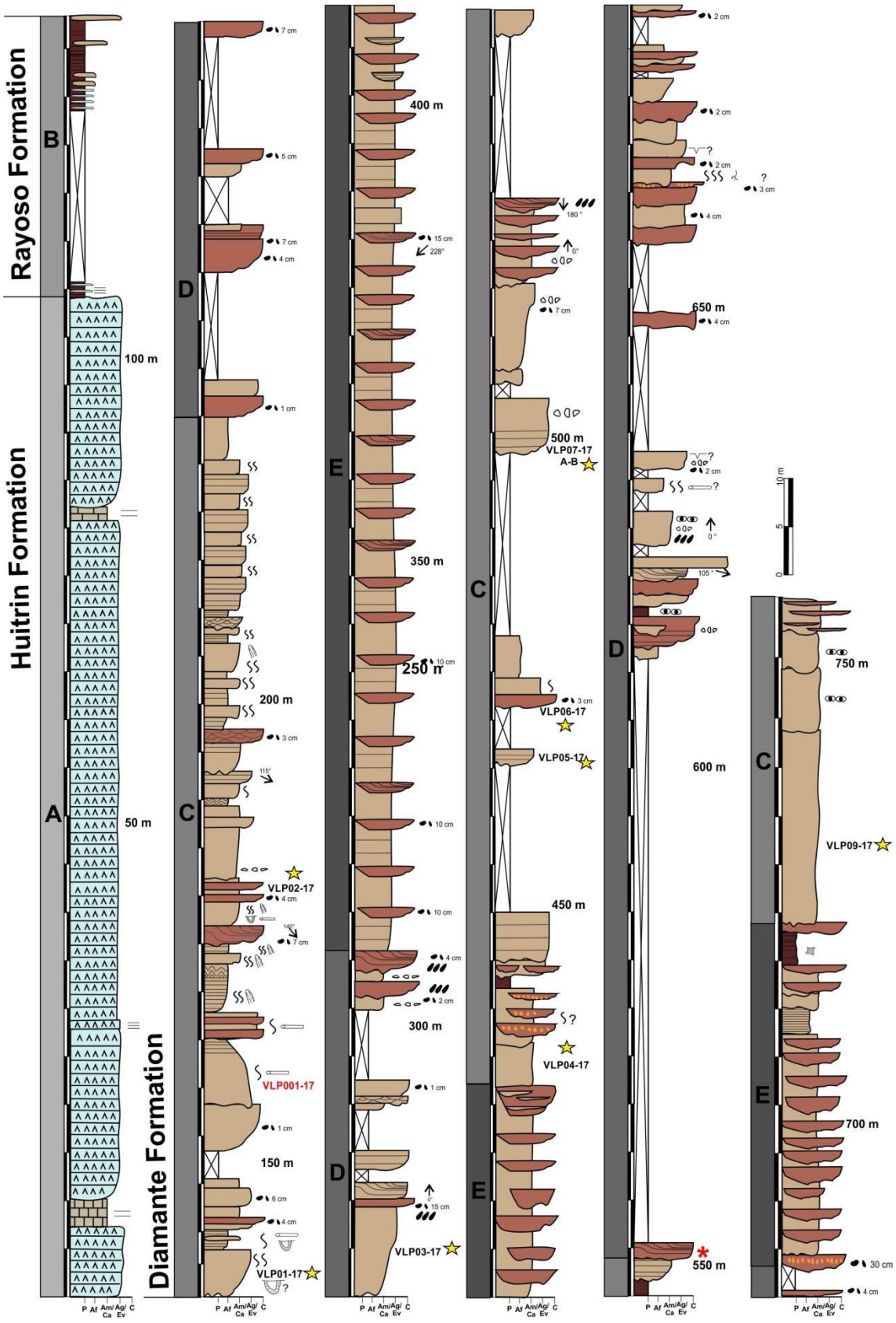
Rayoso Formation
Huitrin Formation
Diamante Formation
A
B
C
D
E
100 m
50 m
200 m
150 m
400 m
350 m
250 m
300 m
500 m
450 m
600 m
650 m
550 m
750 m
700 m
VLP02-17
VLP001-17
VLP01-17
VLP03-17
VLP07-17
A-B
VLP06-17
VLP05-17
VLP04-17
VLP09-17
P Af Am/Ca Ag/Ev C

Figure 5

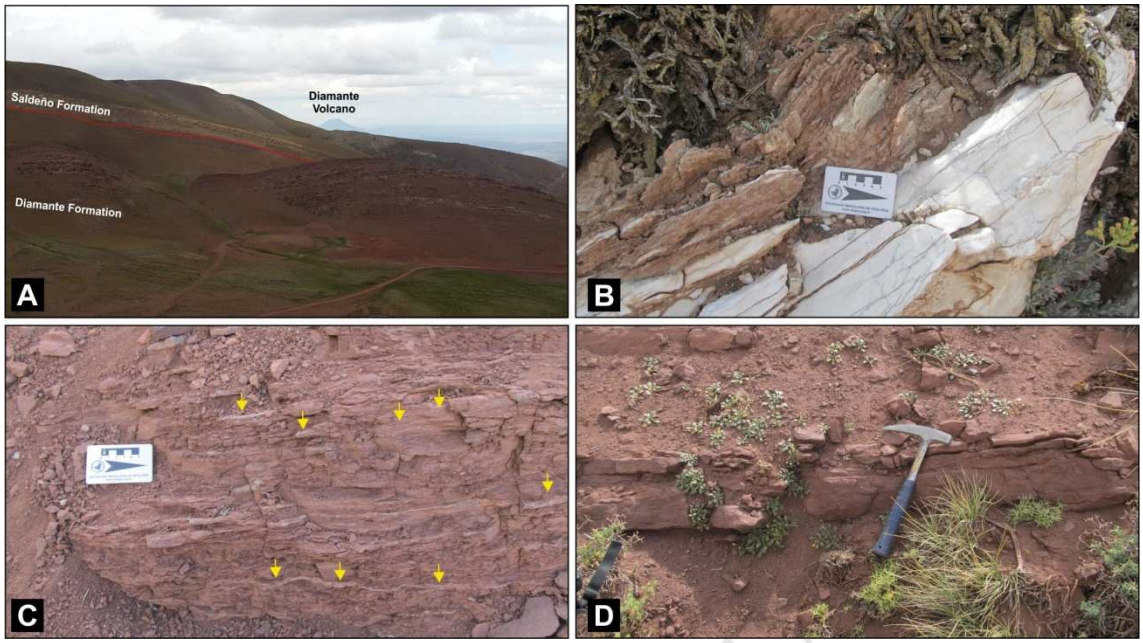

Figure 6

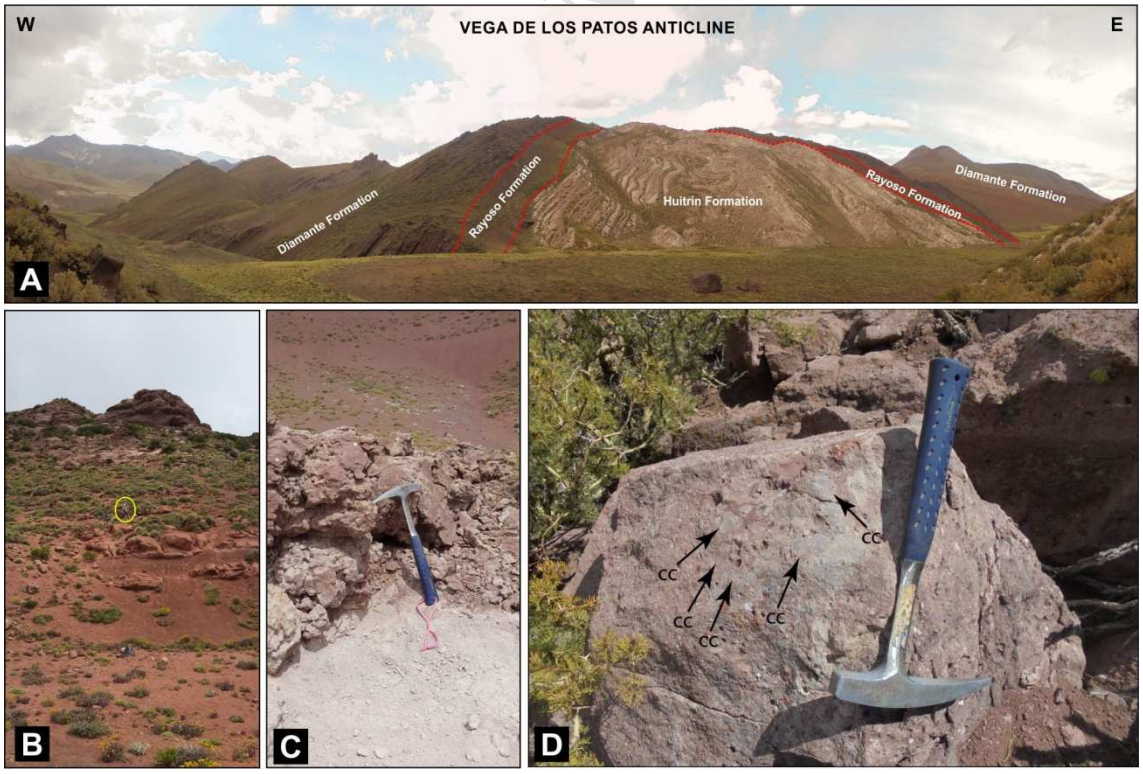

Figure 7

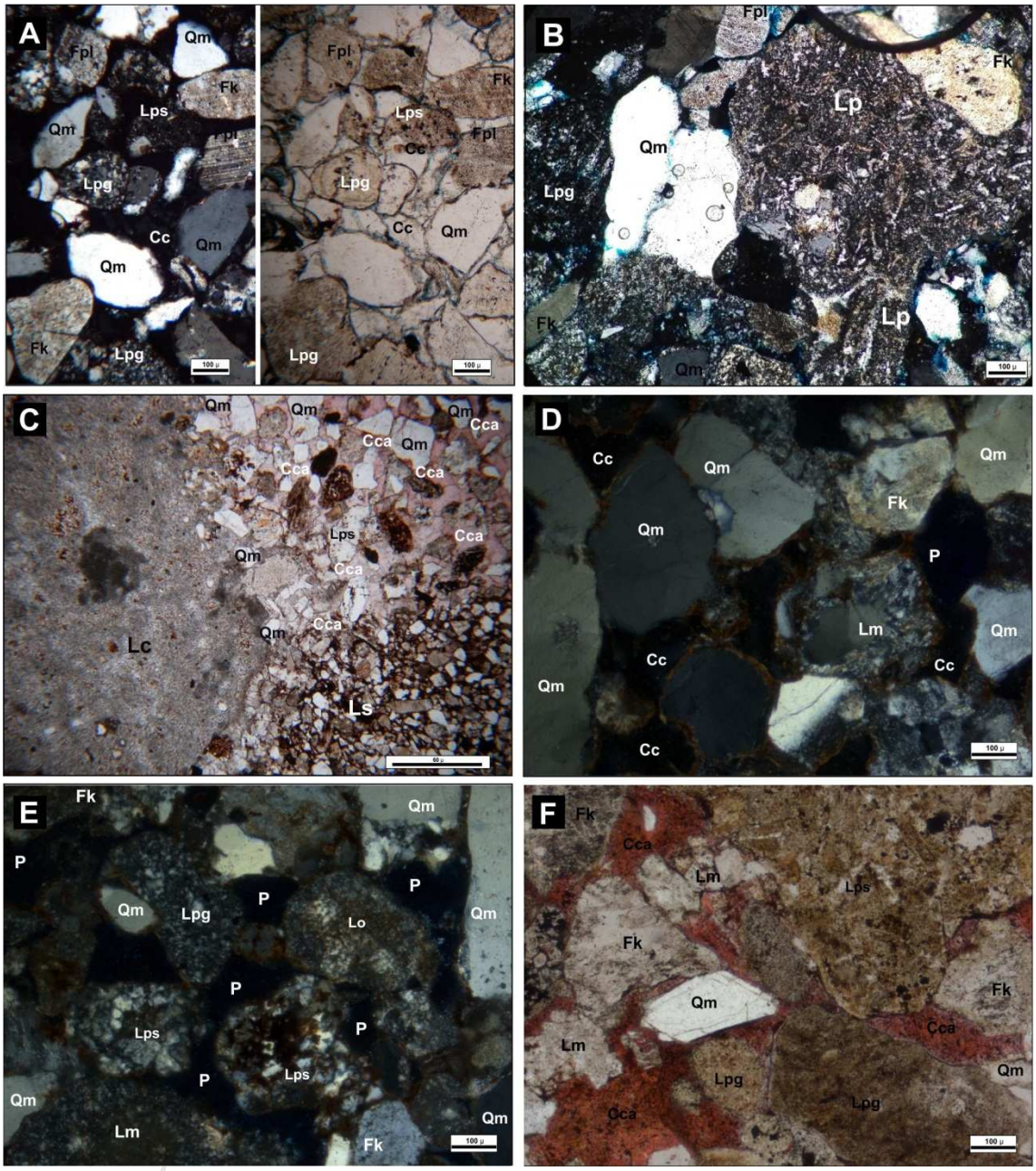
A
Fpl
Qm
Fk
Lps
Qm
Lpg
Cc
Qm
Qm
Fk
Lpg
Fpl
Fk
Lps
Fpl
Cc
Lpg
Cc
Qm
Lpg
B
Fpl
Fk
Lp
Qm
Lpg
Fk
Lp
Qm
C
Qm
Qm
Qm
Cca
Cca
Qm
Cca
Cca
Lps
Cca
Qm
Cca
Qm
Cca
Lc
Ls
D
Cc
Qm
Qm
Fk
Qm
P
Lm
Qm
Cc
Cc
Qm
Cc
E
Fk
Qm
P
P
Qm
Lpg
P
Lo
Qm
P
Lps
P
Lps
P
Qm
Lm
Fk
Qm
F
Fk
Cca
Lm
Lps
Fk
Fk
Qm
Cca
Lm
Qm
Lpg
Lpg
Cca

Figure 8

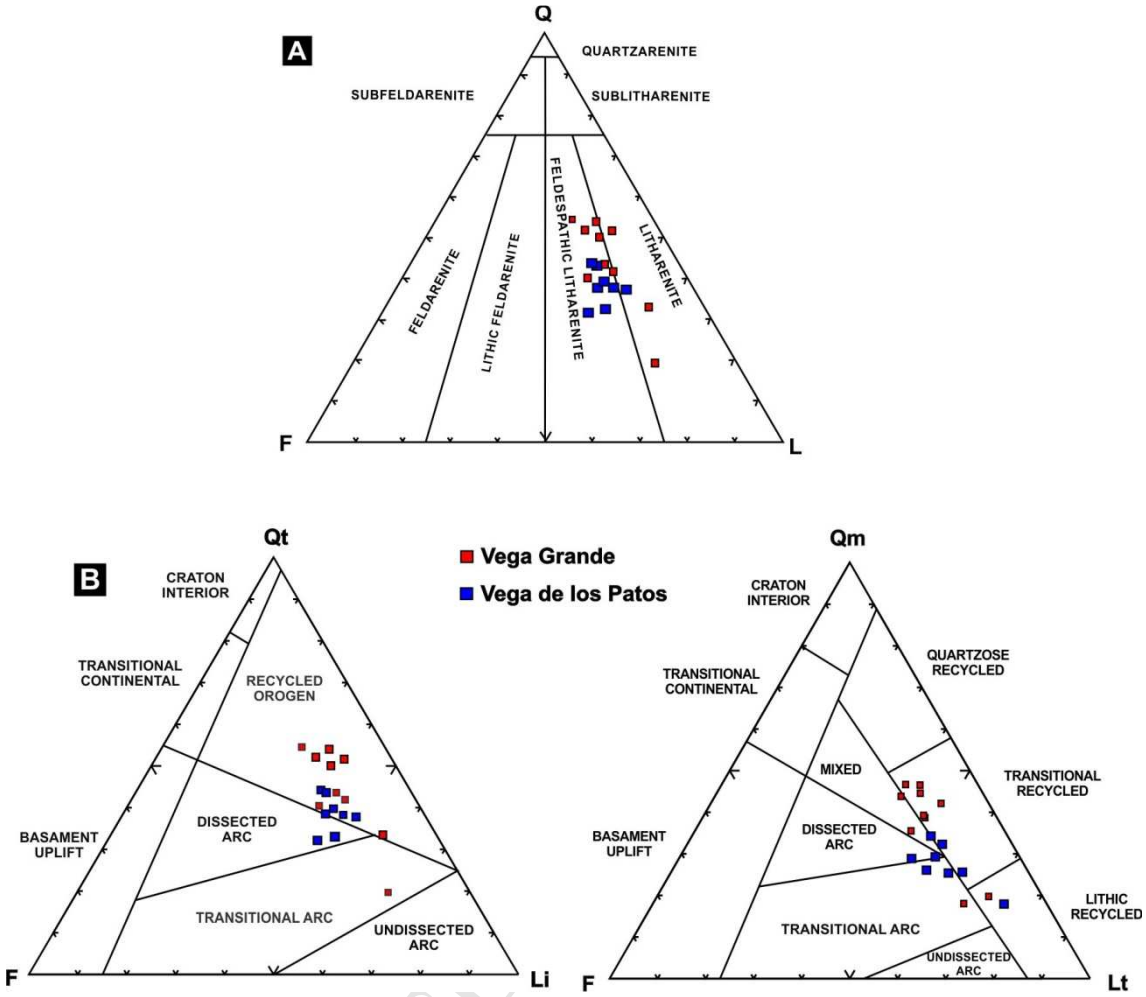

ACCEPTED MANUSCRIPT

Figure 9

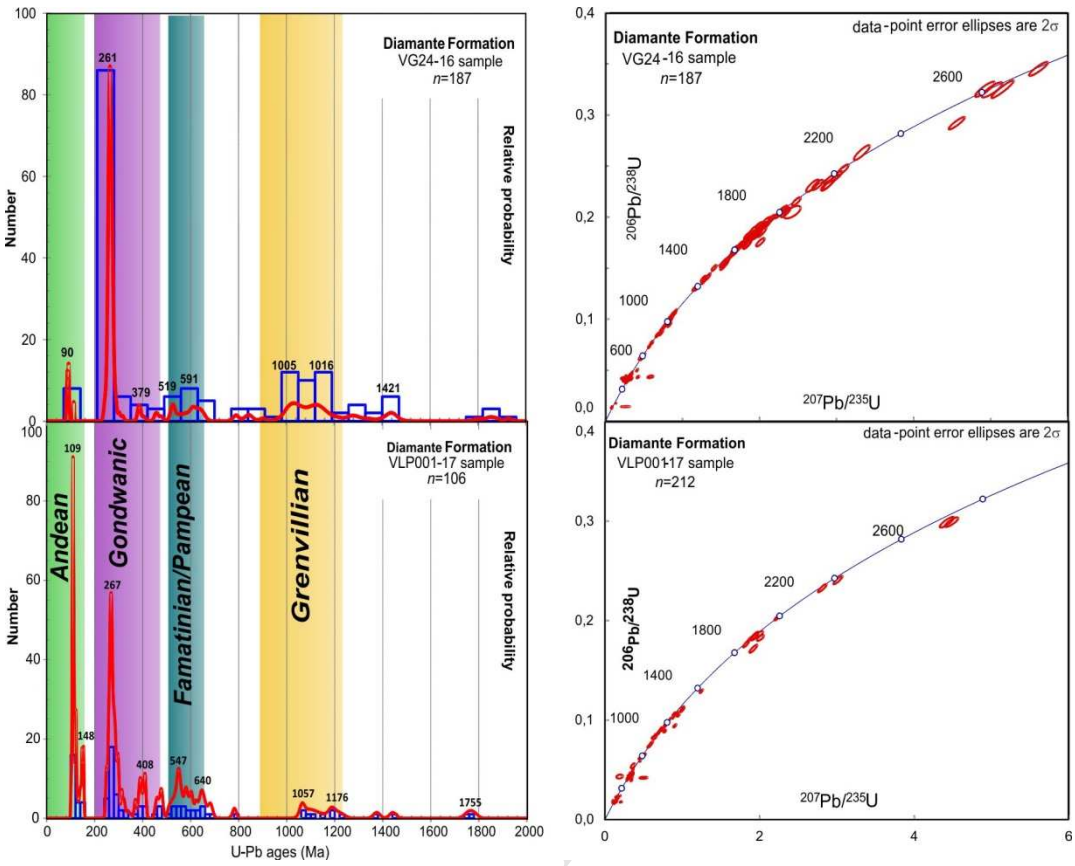

ACCEPTED MANUSCRIPT

Figure 10

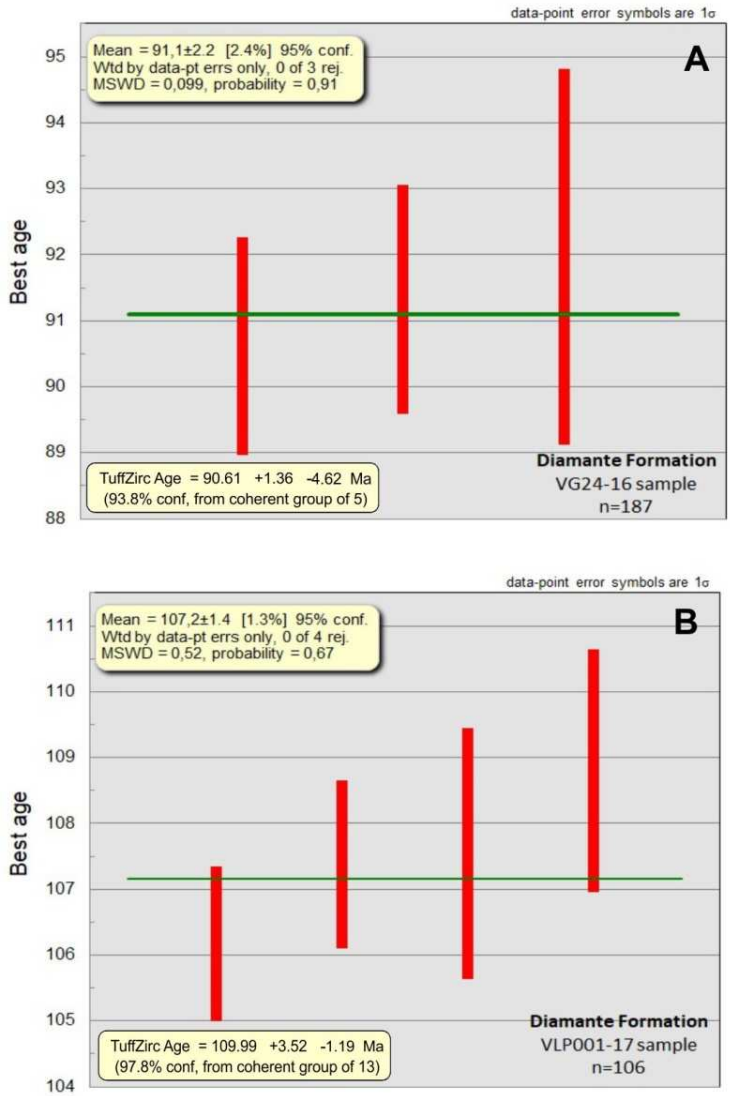

Table 1

	Percentage (%)							
Sample	A	B	C	D	E	F	G	H
VG24-16	4	50	4	11	20	7	3	1
VPL001-17	23	32	9	21	8	1	3	3

ACCEPTED MANUSCRIPT

HIGHLIGHTS

References of manuscript: **SAMES_2019_42**

Title of manuscript: **Onset of foreland basin deposition in the Neuquén Basin (34°-35°S): new data from sedimentary petrology and U-Pb dating of detrital zircons from the Upper Cretaceous non-marine deposits**

- The petrographic analysis shows that the sandstones of the Diamante Formation are mainly feldspatic litharenites and minor litharenites. The source areas are recycled orogen and transitional recycled.
- The variations in the U-Pb age patterns were probably associated with an increase in the volcanic activity in the beginning of the Late Cretaceous and the Andean exhumation during Albian to Campanian times.
- The presence of limestone fragments with ammonites in conglomerates from both study areas suggest provenance from the western Andean orogen
- The maximum depositional ages of Diamante Formation (34-35°S) are 107.2±1.4 Ma and 91.1±2.2 Ma.
- The data shows an evidence of the diachronism in Andean uplift, indicating that the uplift of the Andes started earlier in the northern sector of the Neuquén Basin.

ACCEPTED MANUSCRIPT